Remote Sensing of Environment xxx (2015) xxx–xxx

Contents lists available at ScienceDirect

Remote Sensing of Environment

journal homepage: www.elsevier.com/locate/rse

Differentiating plant species within and across diverse ecosystems with imaging spectroscopy

Keely L. Roth [a,*], Dar A. Roberts [b], Philip E. Dennison [c], Michael Alonzo [b], Seth H. Peterson [b], Michael Beland [b,d]

[a] Department of Land, Air and Water Resources, University of California, Davis, One Shields Ave, Davis, CA 95616, United States
[b] Department of Geography, University of California, Santa Barbara, 1832 Ellison Hall, Santa Barbara, CA 93106, United States
[c] Department of Geography and Center for Natural and Technological Hazards, University of Utah, 260 S Central Campus Dr., Room 270, Salt Lake City, UT 84112, United States
[d] Department of Geography, San Diego State University, 5500 Campanile Dr., Geography Annex 123, San Diego, CA 92182, United States

ARTICLE INFO

Article history:
Received 10 June 2014
Received in revised form 10 May 2015
Accepted 15 May 2015
Available online xxxx

Keywords:
Plant species classification
Hyperspectral
Imaging spectroscopy
AVIRIS
MESMA
Discriminant analysis

ABSTRACT

Imaging spectroscopy has been used successfully to map species across diverse ecosystems, and with several spaceborne imaging spectrometer missions underway (e.g., Hyperspectral Infrared Imager (HyspIRI), Environmental Mapping and Analysis Program (EnMAP)), these data may soon be available globally. Still, most studies have focused only on single ecosystems, and many different classification strategies have been used, making it difficult to assess the potential for mapping dominant species on a broader scale. Here we compare a number of classification approaches across five contrasting ecosystems containing an expansive diversity of species and plant functional types in an effort to find a robust strategy for discriminating among dominant plant species within and across ecosystems. We evaluated the performance of combinations of methods of training data selection (stratified random selection and iterative endmember selection (IES)), spectral dimension reduction methods (canonical discriminant analysis (CDA) and partial least squares regression (PLSR)) and classification algorithms (linear discriminant analysis (LDA) and Multiple Endmember Spectral Mixture Analysis (MESMA)). Accuracy was assessed using an independent validation data set. Mean kappa coefficients for all strategies ranged from 0.48 to 0.85 for each ecosystem. Maximum kappa values and overall accuracies within each ecosystem ranged from 0.56 to 0.90 and 61–92%, respectively. Our findings show that both LDA and MESMA are able to discriminate among species to a high degree of accuracy in most ecosystems, with LDA performing slightly better. Spectral dimension reduction generally improved these results, particularly in conjunction with MESMA. Within each ecosystem, both the number and identities of functional types present, as well as the spatial distribution of dominant species, played a strong role in classification accuracy. In a pooled ecosystem classification, using CDA and LDA, we discriminated among 65 classes with an overall accuracy of 70% for the validation library, using only a 6% training sample. Our results suggest that a spaceborne imaging spectrometer such as HyspIRI will be able to map dominant plant species on a broader scale.

1. Introduction

Accurate information regarding the composition and distribution of dominant plant species and, therefore, plant functional types, within and across ecosystems is pertinent to many research agendas within ecosystem science and plant ecology. Species maps allow scientists to detect the presence or absence of target species (e.g., invasive species, He, Rocchini, Neteler, & Nagendra, 2011; Somers & Asner, 2012) and monitor landscape-scale biological changes such as distribution shifts (Asner, Jones, Martin, Knapp, & Hughes, 2008), type conversion, and disturbance impact and recovery (Hatala, Crabtree, Halligan, & Moorcroft, 2010; Riano et al., 2002). This information is also critical for further refining estimates of ecosystem function (e.g., biomass, habitat suitability), and thus providing improved spatially explicit inputs for evolving ecosystem process and climate models (Goodenough et al., 2006; Kokaly, Asner, Ollinger, Martin, & Wessman, 2009; Ustin, Roberts, Gamon, Asner, & Green, 2004).

Improvements in sensor technology and the development of more sophisticated classification algorithms have enabled remote sensing scientists to discriminate among various vegetation communities (e.g., forest, crop, grassland) and life forms (e.g., herbaceous, shrubs, trees) (DeFries, Hansen, & Townshend, 1995; Friedl et al., 2010), between different leaf types (i.e., broadleaf vs. coniferous) (Van Aardt & Wynne, 2001) and among plant functional types (PFTs) (e.g., deciduous broadleaf tree, evergreen needleleaf shrub) (reviewed in Ustin & Gamon, 2010). However, discriminating individual plant species requires data with fine spectral resolution, which can be acquired using imaging spectrometers (Clark,

---

[*] Corresponding author.
E-mail address: klroth@ucdavis.edu (K.L. Roth).

http://dx.doi.org/10.1016/j.rse.2015.05.007

Please cite this article as: Roth, K.L., et al., Differentiating plant species within and across diverse ecosystems with imaging spectroscopy, *Remote Sensing of Environment* (2015), http://dx.doi.org/10.1016/j.rse.2015.05.007

Roberts, & Clark, 2005). Imaging spectrometers are sensitive to subtle shifts in spectral properties that are controlled by leaf biochemistry, anatomy and physiology and are further modified by canopy architecture (Asner, 1998; Roberts et al., 2004). As such, these instruments have been used successfully to discriminate among plant species and functional types using leaf-level observations (Castro-Esau, Sanchez-Azofeifa, & Caelli, 2004; Clark et al., 2005), field-collected canopy spectra (Gong, Pu, & Yu, 1997; Pu, 2009), and image data (Martin, Newman, Aber, & Congalton, 1998; Van Aardt & Wynne, 2007). Indeed, a major aim of several upcoming global hyperspectral missions is to map plant species and functional types in support of ecosystem research, including NASA's Hyperspectral Infrared Imager (HyspIRI; HyspIRI Team, 2009). HyspIRI would collect full Visible/Near-Infrared/Short-wave infrared (VNIR-SWIR) spectra (400–2500 nm) at 60 m spatial resolution on a global, 19 day repeat cycle.

The ability to discriminate accurately among dominant plant species and PFTs on regional to global scales represents a major advance in remote sensing science (Asner, 2013). However, success depends, in large part, on a solid understanding of the spectral, spatial and temporal resolution constraints on mapping species within and across a diverse set of ecosystems. Indeed, most imaging spectroscopy studies have sought to measure the spectral separability of, or to classify, species in single ecosystems or species in single plant functional types (e.g., Féret & Asner, 2012a; Kalacska, Bohlman, Sanchez-Azofeifa, Castro-Esau, & Caelli, 2007; Pu, 2009; Vaiphasa, Ongsomwang, Vaiphasa, & Skidmore, 2005; Van Aardt & Wynne, 2007) and thus have investigated a limited diversity of species and functional types, making comparisons across ecosystems challenging. Furthermore, most studies that explicitly evaluate the effects of dimension reduction (Dópido et al., 2012; Kalacska et al., 2007; Pu & Gong, 2000) or classification method (Clark et al., 2005; Féret & Asner, 2012b) on classification accuracy, have performed such analyses on only a single test data set or within a single ecosystem, or do not focus on discriminating among plant species. None, to our knowledge, evaluate the impact of different combinations of methods across a diversity of ecosystems.

To fully leverage the data provided by a global imaging spectrometer, such as HyspIRI, we must improve our understanding of the spectral properties of a diverse range of species and PFTs in the landscapes we seek to map, the methods we use to create these maps and how the two interrelate. Thus, the goals of this research were to evaluate our ability to spectrally discriminate dominant plant species in contrasting ecosystems and to compare the performance of several hyperspectral classification strategies in accurately mapping species across multiple, diverse ecosystems. Our main research questions are as follows:

1) Within individual ecosystems, how spectrally separable are the dominant species and what ecosystem characteristics drive observed separability?
2) When applied to a diverse set of ecosystems, how do classification strategies differ in performance, i.e. is there a clearly superior strategy?
3) What is the potential for differentiating among species from all ecosystems using the best approach as determined by question 2?

Comparing different classification approaches across ecosystems, we can evaluate if (and how) the methods perform differently for different ecosystems. This will indicate if there is a best overall approach, or if different approaches are needed depending on the ecosystem. By applying the same classification methods at each site, we highlight our ability to spectrally separate species in each ecosystem type. In other words, we can characterize what makes one ecosystem easier to map vs. another, and explore the possibility of a general limit to how accurately dominant species within a particular ecosystem type can be classified with imaging spectroscopy data alone. By combining the ecosystems, we are testing our ability to map species across multiple ecosystems simultaneously, which will be the goal for the larger footprint spaceborne hyperspectral data collected by a sensor like HyspIRI. Does such a classification yield acceptable results? How are class-level accuracies affected (e.g., are some species classified more accurately with higher diversity in the classification? are species within the same plant functional type but from different ecosystems spectrally confused?)? Do we see similar patterns in misclassification when all sites are grouped together as we do when we map sites individually? The answers to these questions can provide great insight for future large scale species mapping efforts.

2. Methods

2.1. Study sites & data collection

We analyzed image data from five different North American ecosystems (Fig. 1, Table 1). The Smithsonian Environmental Research Center (SERC) site is a temperate, broadleaf deciduous forest in eastern Maryland ranging in elevation from 2 to 20 m. It is dominated by intermediate to mature stands of tulip poplar (*Liriodendron tulipifera*) and sweetgum (*Liquidambar styraciflua*) mixed with maple (*Acer* spp.), hickory (*Carya* spp.) and beech (*Fagus* spp.). The forested area of the site is surrounded primarily by agriculture and open fields. The Gulf study site is located in coastal Louisiana, including Barataria Bay and the Mississippi delta, with elevations just above sea level. It is a marsh ecosystem strongly influenced by a subtropical climate and the confluence of fresh and salt water. Cordgrass (*Spartina* spp.), Salt grass (*Distichlis spicata*), and black rush (*Juncus roemerianus*) dominate the salt and brackish marsh zones, and common reed (*Phragmites australis*) becomes prevalent in intermediate to fresh water zones. The Wind River Experimental Forest (WR) site is a mixed broadleaf and coniferous temperate rainforest located in southern Washington in the Cascade Mountains, covering an elevation gradient of approximately 250 to 800 m. It is dominated primarily by western hemlock (*Tsuga heterophylla*) and Douglas fir (*Pseudotsuga menziesii*), with an herbaceous understory and smaller stands of maple (*Acer* spp.), cottonwood (*Populus trichocarpa*) and alder (*Alnus rubra*). The Sierra Nevada site (SNEV) is a mixed montane coniferous forest in the southern Sierra Nevada Mountains of California. The site includes major portions of the Sierra National Forest, extending from Shaver Lake southeast to Kings Canyon National Park and covering a range in elevation from approximately 1200 to 2000 m. It is composed of large mixed stands of fir (both white and red, *Abies concolor* and *magnifica*, respectively) and pine (Ponderosa, Jeffrey and sugar; *Pinus ponderosa*, *jeffreyi*, and *lambertiana*, respectively), as well as broad swaths of deciduous and evergreen oak (*Quercus kelloggii* and *Quercus chrysolepsis*, respectively) with shrub-dominated rocky outcrops, open meadows and riparian zones. The Santa Barbara (SBFR) site runs east to west along the front range of the coastal Santa Ynez Mountains in southern California, and extends north from Santa Barbara into the San Raphael Mountains. It covers a large swath of shrublands, grasslands, woodlands and urban areas distributed over 1 to 1366 m elevation, and has a Mediterranean climate, with cool, moist winters and dry, warm summers. Wooded regions are dominated by oak (*Quercus* spp.) and California bay laurel (*Umbellularia californica*), with some patches of sycamore (*Platanus racemosa*) and gray pine (*Pinus sabiniana*). Major chaparral shrub species include *Ceanothus* spp., chamise (*Adenostoma fasciculatum*), and manzanita (*Arctostaphylos* spp.).

Image data were acquired by the Airborne Visible/Infrared Imaging Spectrometer (AVIRIS) over the five study regions (Table 1). AVIRIS collects data in 224 bands from 350 to 2500 nm with a full-width, half-maximum of about 10 nm (Green et al., 1998). Data were preprocessed to radiance and georectified using a ray tracing algorithm with a digital elevation model (Boardman, 1999). Reflectance was retrieved for all images using either MODTRAN-derived look-up tables for path and reflected radiance (described in Roberts, Green, & Adams, 1997), ACORN (ImSpec LLC) or ATCOR-4 (Richter & Schläpfer, 2002). Bands with low signal to noise ratio and/or high levels of atmospheric

Please cite this article as: Roth, K.L., et al., Differentiating plant species within and across diverse ecosystems with imaging spectroscopy, *Remote Sensing of Environment* (2015), http://dx.doi.org/10.1016/j.rse.2015.05.007

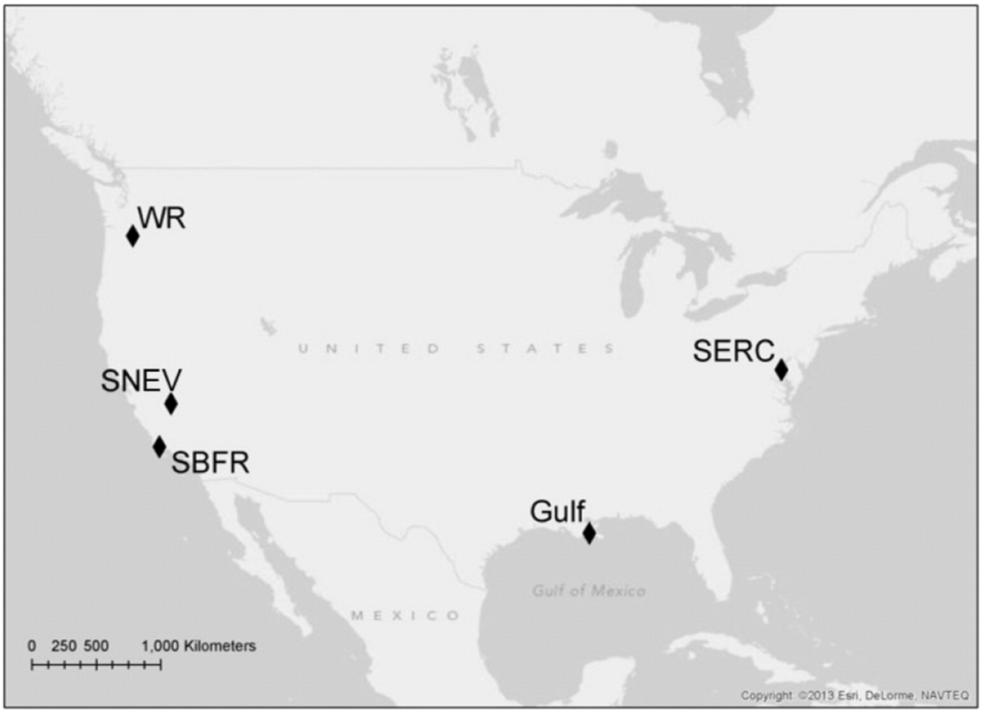

Fig. 1. Locations of the five study sites. The Wind River (WR) site is in southern Washington. The Sierra Nevada (SNEV) site is in the southern portion of the Sierra National Forest in California. The Santa Barbara site (SBFR) is on the southern central coast of California. The Gulf site (Gulf) is on the coast of Louisiana. The Smithsonian Environmental Research Center (SERC) site is in eastern Maryland.

contamination were removed. Images were further georectified using high resolution Digital Orthophoto Quarter Quads (DOQQs). Spatial resolution varied from 3.3 m to 18 m across sites, and acquisition dates were timed to capture peak productivity (Table 1). Between 1 and 8 flight lines were analyzed for each site, bringing the total analysis coverage to ~11,000 km^2. It should be noted that a substantial portion of this area was from the Gulf site and included large areas of open water.

For each site, reference data were collected in the field or using available geospatial data to identify the most common dominant species and cover types. Reference patches (polygons) composed of 70% or more of the dominant species or cover type were collected for each site. At SERC, polygons were delineated on the AVIRIS imagery using a detailed inventory covering our area of interest provided by the Smithsonian Environmental Research Center for tree species and using high resolution aerial photos for crop and soil cover classes. For tree species, we delineated any patch greater than 2 pixels (4 × 8 m) in size. At WR, SBFR, and SNEV, patches were identified in the field using a long distance visual estimation technique (Meentemeyer, Moody, & Franklin, 2001) or by walking areas on foot to estimate composition. Target patch size for SNEV and SBFR was 120 × 120 m. At the Gulf site, reference patches were created based on visual estimates made via a helicopter survey, as well as previously existing species occurrence maps (Sasser, Visser, Mouton, Linscombe, & Hartley, 2008). In all cases, we sought to collect at least 10 patches with high purity per class, though this was not possible for all species and cover types. The total number of reference polygons collected for each site ranged from 79 (SNEV) to 385 (SBFR). Aggregating the sites, the reference polygon set encompasses 10 distinct PFTs (including 42 species, 9 genera and 6 plant communities) and 3 additional common cover types (e.g., rock) (Table 2). Site-specific spectral libraries were extracted from the image data for all pixels falling within these reference patches. Full spectral libraries contained as few as 3442 to as many as 44,325 spectra (Table 2).

2.2. Classification strategies

2.2.1. Training data selection

For supervised classification, both a training data set composed of a representative sample of each class in the analysis and an independent validation data set are needed. Frequently, there are not enough reference data available to properly validate species classifications, and in some cases, a bootstrapping or cross-validation approach is used (Isaksson et al., 2008). When enough reference data are available, training data selection generally includes random sampling of reference patches (i.e., setting aside some patches for training and some for validation). However, this can result in very unbalanced and/or biased training datasets, depending on the number, size and spatial distribution of patches present for each species, which will likely influence classification accuracy (Congalton, 1991). Roth, Dennison, and Roberts (2012) proposed a stratified random sampling for approach for selecting training data in which spectra for each class are randomly selected from the pool until every reference patch has been sampled to user-defined limits. Thus, each reference patch contributes some pixels to training and the

Table 1
Image acquisition data and classification results by site, class type and resolution.

Site	Lat, lon	Ecosystem	Image acquisition date	Spatial resolution	Approximate coverage (km^2)
SERC	38.9°N, 76.6°W	Temperate, broadleaf, deciduous forest	2006-May-29	3.5 m	24
GULF	29.4°N, 90.0°W	Tidal marsh	2010-May-06	18 m	8996
WR	45.8°N, 122.0°W	Temperate coniferous, broadleaf rainforest	2003-Jul-11	4 m	209
SNEV	37.0°N, 119.3°W	Mixed coniferous, broadleaf montane forest	2003-Jul-18	3.3 m	235
SBFR	34.6°N, 120.1°W	Mediterranean climate shrubland, woodland, grassland	2009-Jun-17	12 m	1516

Please cite this article as: Roth, K.L., et al., Differentiating plant species within and across diverse ecosystems with imaging spectroscopy, *Remote Sensing of Environment* (2015), http://dx.doi.org/10.1016/j.rse.2015.05.007

Table 2
Summary table of plant functional types and dominant species and cover types for each site. Includes reference polygon and spectral library sample sizes.

Plant functional type	Dominant species or cover type	Abbreviation	Polygons	Spectra	Training spectra
SERC			111	9800	906
Annual herbaceous	Crop	CROP	4	2190	40
Senesced annual herbaceous	Crop residue/senesced grass	DGCRP	5	3236	50
Deciduous broadleaf tree	*Acer* spp.	ACSP	13	214	93
	Carya spp.	CASP	19	333	142
	Fagus spp.	FASP	15	396	133
	Liquidambar styraciflua	LIST	10	241	84
	Liriodendron tulipifera	LITU	16	1702	150
	Platanus occidentalis	PLOC	5	38	17
	Quercus spp.	QUSP	13	251	111
Evergreen needleleaf tree	*Pinus* spp.	PISP	6	74	36
n/a	Bare soil	SOIL	5	1125	50
GULF			141	3442	1165
Evergreen broadleaf shrub	*Avicennia germinans*	AVGE	10	251	87
Perennial herbaceous	*Distichlis spicata*	DISP	16	325	135
	Juncus roemerianus	JURO	3	377	30
	Phragmites australis	PHAU	26	787	237
	Spartina alterniflora	SPAL	60	925	430
	Spartina patens	SPPA	17	490	168
Senesced vegetation	Senesced vegetation	OILED	1	7	3
n/a	Clear water	CWTR	1	44	10
	Dark water	DWATER	2	90	20
	Sun glint	GLINT	3	78	25
	Muddy water	MWTR	2	68	20
WR			134	23,886	1047
Senesced annual herbaceous	Senesced grass	DGRASS	15	3639	147
Deciduous broadleaf shrub	*Acer circinatum*	ACCI	6	55	23
Deciduous broadleaf tree	*Acer macrophyllum*	ACMA	10	374	80
	Alnus rubra	ALRU	27	1299	225
	Populus trichocarpa	POTR	12	1005	96
Evergreen needleleaf tree	Abies grandis	ABGR	2	20	9
	Pseudotsuga menziesii	PSME	30	9406	286
	Thuja plicata	THPL	11	85	35
	Tsuga heterophylla	TSHE	8	7856	80
Perennial herbaceous	*Pteridium aqualinum*	PTAQ	10	78	36
n/a	Rock or soil	ROCK-SOIL	3	69	30
SNEV			79	44,325	790
Deciduous broadleaf tree	*Quercus kelloggii*	QUKE	5	3771	50
	Salix spp.	SASP	1	228	10
Evergreen broadleaf shrub	*Arctostaphlyos* spp.	ARSP	11	3451	110
	Ceanothus cordulatus	CECO	2	848	20
Evergreen broadleaf tree	*Quercus chrysolepsis*	QUCH	3	993	30
Evergreen needleleaf tree	*Abies concolor*	ABCO	16	10,956	160
	Abies magnifica	ABMA	6	2386	60
	Calocedrus decurrens	CADE	4	1033	40
	Pinus jeffreyi	PIJE	2	1894	20
	Pinus lambertiana	PILA	6	745	60
	Pinus ponderosa	PIPO	11	10,071	110
	Sequoiadendron giganteum	SEGI	2	91	20
Annual herbaceous	Mixed meadow	MEADOW	6	5069	60
n/a	Rock	ROCK	4	2789	40
SBFR			385	39,946	3749
Annual herbaceous	Irrigated grasses	IRGR	16	1063	160
Senesced annual herbaceous	*Brassica nigra*	BRNI	15	2573	150
	Mediterranean annual grasses and forbs	MAGF	20	4305	199
Deciduous broadleaf tree	*Platanus racemosa*	PLRA	15	2032	150
	Quercus douglasii	QUDO	17	2232	170
Drought-deciduous shrub	*Artemisia californica–Salvia leucophylla*	ARCA-SALE	15	2027	150
Evergreen broadleaf shrub	*Arctostaphylos* spp.	ARSP	20	2191	199
	Baccharis pilularis	BAPI	15	560	127
	Ceanothus cuneatus	CECU	13	777	129
	Ceanothus megacarpus	CEME	27	2254	264
	Ceanothus spinosus	CESP	14	1219	140
Evergreen broadleaf tree	*Citrus* spp.	CISP	15	766	119
	Eucalyptus spp.	EUSP	15	1845	150
	Persea americana	PEAM	17	1134	170
	Quercus agrifolia	QUAG	15	1189	150
	Umbellularia californica	UMCA	15	1147	147
Evergreen needleleaf shrub	*Adenostoma fasciculatum*	ADFA	32	2670	320
	Eriogonum fasciculatum	ERFA	15	2074	150
Evergreen needleleaf tree	*Pinus sabiniana*	PISA	15	1455	145
Perennial herbaceous	Marsh/wetland	MARSH	16	2798	160
n/a	Rock	ROCK	13	598	123
	Bare soil	SOIL	15	1064	127
	Urban land use	URBAN	15	1973	150

Please cite this article as: Roth, K.L., et al., Differentiating plant species within and across diverse ecosystems with imaging spectroscopy, *Remote Sensing of Environment* (2015), http://dx.doi.org/10.1016/j.rse.2015.05.007

remainder to validation, resulting in a more balanced training dataset across classes and a validation dataset that is representative of the real-world class frequency.

Another option for selecting training data includes the further sub-selection of endmember libraries from the training sample. This is common practice when using multiple endmember spectral mixture analysis (MESMA) for either classification or fractional cover modeling (Dennison & Roberts, 2003b; Roberts et al., 2012). Using a smaller subset of reference data for training can have several advantages. It leaves a greater portion of the reference data available for validation. Sub-selecting the most representative endmembers for each class may also improve accuracy and reduce classification time which is an important advantage when using an iterative classifier like MESMA. Many methods exist to select endmembers from a reference spectral library (Dennison et al., 2004), but one developed specifically for classification is Iterative Endmember Selection (IES) (Schaaf, Dennison, Fryer, Roth, & Roberts, 2011). In IES, spectra are added and subtracted from the endmember library in a stepwise procedure until the highest within-library kappa is reached across classes (Roth et al., 2012; Schaaf et al., 2011). The kappa coefficient is a measure of how well a classification separates classes, which takes into account accuracy due to random chance (Congalton, 1991) While the libraries produced by IES can be quite large, they represent a quantitative selection method for subsetting an even larger library to select training data.

In our study, the spectral libraries for each site were randomly sampled into training and validation libraries using the method defined in Roth et al. (2012). Here, we limited the number of spectra from each reference polygon to either 50% of the pixels in the polygon or 10 spectra total, whichever was less. Overall, this sampling approach leads to a relatively small proportion of the spectra being used as training data. IES was then applied to this training library to select a second training data set for each site, referred to hereafter as the 'IES library'.

2.2.2. Dimension reduction

Dimension reduction techniques (sometimes called feature extraction) seek to address band collinearity while maximizing the variance of the entire data set, or, when applied for classification, the between-group variance (Yeh & Spiegelman, 1994). Dimension reduction techniques such as principal components analysis (PCA; Pu and Gong (2000)) minimum noise fraction (MNF; Plourde, Ollinger, Smith, and Martin (2007)), canonical discriminant analysis (CDA; Alonzo, Roth, and Roberts (2013)) and partial least squares regression (PLSR; Wold, Sjostrom, & Eriksson, 2001) can simultaneously improve accuracies and computational efficiency when classifying large datasets. In this study, we focus on two particularly promising dimension reduction methods which, to date, have not been widely used in remote sensing science for classification: CDA and partial least squares regression (PLSR) (Pu & Gong, 2011). CDA, also known as multiple linear discriminant analysis, is one of the most commonly used dimensionality reduction techniques for a broad range of classification problems (e.g., pattern recognition and chemometrics). Similar to PCA, CDA is used to derive canonical variates, which are linear combinations of the original variables. In contrast to PCA, these functions are created to maximize the between-group variance rather than to maximize variance in the entire dataset (Klecka, 1980; Zhao & Maclean, 2000). The number of functions (set of eigenvectors) derived from CDA is limited to the number of classes minus one or the number of observed variables, whichever is fewer. Each discriminant function comprises a set of standardized coefficients (one per band). When these functions are multiplied through the original spectral data, they yield a reduced set of spectra with the same number of bands as functions. One clear advantage of CDA dimension reduction is that it allows for interpretation of the derived coefficients after standardization (Alonzo et al., 2013; Klecka, 1980). In other words, researchers are able to analyze the relationships between bands and the discriminant functions, something that cannot be done with simple LDA coefficients. CDA, does, however, require a minimum number of training samples per class, such that the estimated W matrix is positive definite.

The second dimension reduction technique used in this study is PLSR. PLSR was not originally developed for discrimination of classes, but as an econometric modeling technique for over-determined regression models, and it soon became widely used in chemometric and spectrometric modeling (Boulesteix & Strimmer, 2006). This is, in part, because PLSR is well-suited for data with small training sample sizes relative to a large numbers of predictor variables. PLSR simultaneously models both the structure of the predictor variables (here spectral bands) and the response variables (here class membership). The resulting coefficient matrix represents the covariance structure between the two. The application of these coefficients to the spectral data is the same as in CDA, yielding a reduced set of variables with the same number of bands as PLS components. These reduced data can then be used in a classifier. In remote sensing, PLSR has not been used for species discrimination, but it has been widely applied for predicting plant biochemistry (e.g., chlorophyll, carotenoids, nitrogen, etc.) (Asner & Martin, 2008; Asner, Martin, Anderson, & Knapp, 2015; Martin, Plourde, Ollinger, Smith, & McNeil, 2008; Zhai et al., 2013) and even photosynthetic metabolism (Serbin, Dillaway, Kruger, & Townsend, 2012). The main advantage of PLSR over CDA as a dimension reduction technique is that PLSR does not require a minimum training sample size. This can be critical when working with fewer reference spectra than spectral bands.

To reduce the dimensionality of our spectra, CDA coefficients for each site were calculated using the full training library. We did not derive CDA coefficients using the IES library due to its requirement for a greater number of class observations than variables. PLSR coefficients were calculated for both training and IES libraries because PLSR can estimate coefficients in cases with more variables than observations. For both CDA and PLSR dimension reduction, the number of functions or components derived was set equal to the number of classes minus one. This is the maximum number of functions that can be derived using CDA. The CDA coefficients and both sets of PLSR coefficients were multiplied through the appropriate libraries to transform the spectra into CDA or PLSR variables. Coefficient estimation and application was performed using code developed and implemented in MATLAB (The Mathworks Inc., 2012).

2.2.3. Classifiers

We implemented two supervised classification techniques: Fisher's linear discriminant analysis (LDA) and the two endmember case of MESMA. In LDA, data are transformed linearly to maximize the between-class variance relative to within class variance (Fisher, 1936). When used for classification of multiple classes, a single discriminant function is calculated for separating each class from all others (i.e., one against the rest). Class discriminant scores are calculated for each spectrum to be classified, and the spectrum is assigned to the class for which it has the highest score. One advantage of LDA is that it uses a pooled within-class covariance matrix (in contrast to quadratic discriminant analysis, which estimates covariance separately for each class). Because of this, LDA is "less sensitive to ill- and poorly posed problems" (Féret & Asner, 2012b). However, a sufficient number of training samples are needed to ensure a positive definite class covariance matrix. This is often not possible using hyperspectral data where the number of observed variables is high and class sample sizes are often small (Du, 2007; Féret & Asner, 2012b). Studies using LDA have achieved very high classification accuracies at the species level in various ecosystems (Féret & Asner, 2012b; Franklin, 1994; Pu, 2009; Van Aardt & Wynne, 2007).

MESMA is another technique widely applied to mapping species with imaging spectroscopy data. MESMA is an extension of spectral mixture analysis (Roberts, Smith, & Adams, 1993). In SMA, a pixel's spectrum is modeled as a linear combination of pure 'endmember' spectra plus an error term. MESMA is a variation of SMA in which both the

Please cite this article as: Roth, K.L., et al., Differentiating plant species within and across diverse ecosystems with imaging spectroscopy, *Remote Sensing of Environment* (2015), http://dx.doi.org/10.1016/j.rse.2015.05.007

number and type of endmember spectra are allowed to vary per pixel (Roberts et al., 1998). Though primarily used to model fractional cover, the two-endmember case of MESMA can be used to model unknown spectra as linear combinations of shade and a pure 'endmember' spectrum, representative of a class of interest. Using an iterative fitting process, each unknown spectrum is assigned the class of the endmember with the lowest root mean squared error (RMSE) (Dennison & Roberts, 2003a, 2003b). A key advantage to using MESMA for classification is its ability to use the entire spectrum regardless of sample size per class; no dimension reduction techniques are necessary. This approach has been used in montane ecosystems (Schaaf et al., 2011; Swatantran, Dubayah, Roberts, Hofton, & Blair, 2011), forests (Plourde et al., 2007; Roberts, Gamon, Keightley, & Prentiss, 1999; Youngentob et al., 2011), shrublands (Dennison & Roberts, 2003a, 2003b; Roth et al., 2012), and wetlands (Li, Ustin, & Lay, 2005; Rosso, Ustin, & Hastings, 2005; Underwood et al., 2006).

Classifications using both techniques were run using full spectrum, CDA and PLSR libraries, yielding nine unique classification configurations (Fig. 2). These analyses were repeated for each site.

2.2.4. Accuracy assessment & comparative analysis

For each classification configuration, the overall accuracy, kappa, error matrix and class-specific user's and producer's accuracies were calculated. All accuracies reported are for the validation libraries. We compared accuracy metrics within and across sites to both assess the effects of training data selection, dimension reduction, and classifier performance and to evaluate the spectral separability among species within each ecosystem type. Overall accuracies and kappa values were rank transformed, and repeated measures ANOVA was used to determine if significant differences existed among classification configurations by site. Tukey's post-hoc multiple comparisons test with the Holm adjustment was run for all pairs of configurations to determine significant differences. Using IES-selected training spectra resulted in significantly lower accuracies across all sites and in all method combinations, and is not discussed further to simplify our results.

As with most classifications, the success depends on the user requirements. In this study, our aim was to assess the potential to map dominant plant species and functional types at regional to continental scales. Thus, we are seeking a classification strategy having good overall accuracy, acceptably high producer's and user's accuracies for many classes, and improved performance over other approaches, across diverse sites. To assess how well each configuration met these requirements, we generated four performance metrics: 1) the mean percentage of classes from each site having both a producer's and user's accuracy ≥60%; 2) the mean percentage of classes from each site for which the configuration was a top performer in producer's accuracy; 3) the mean percentage of classes from each site for which the configuration was a top performer in user's accuracy; and 4) the mean kappa value of the configuration across sites. Metric 1 represents the proportion of classes at each site that a particular configuration discriminated well. Metrics 2 and 3 indicate how well each configuration performed relative to the others at discriminating individual classes. To identify 'top performers' for each class, we rounded the producer's and user's accuracies to the nearest 5% and identified those configurations with the highest rounded accuracy for a class. Metric 4 indicates overall classification performance of a configuration at each site. For metrics 1–3, we used means so that each ecosystem was given equal weight regardless of the number of classes found there. We then ranked the metrics across classification configurations.

2.3. Combined-ecosystem classification

We merged the spectral libraries from each site to create combined-sites (CS) training, endmember and validation libraries. This allowed us to evaluate the potential for using reference libraries containing spectra acquired on different dates, from several ecosystems, and at varying spatial resolutions to classify dominant plant species and cover types

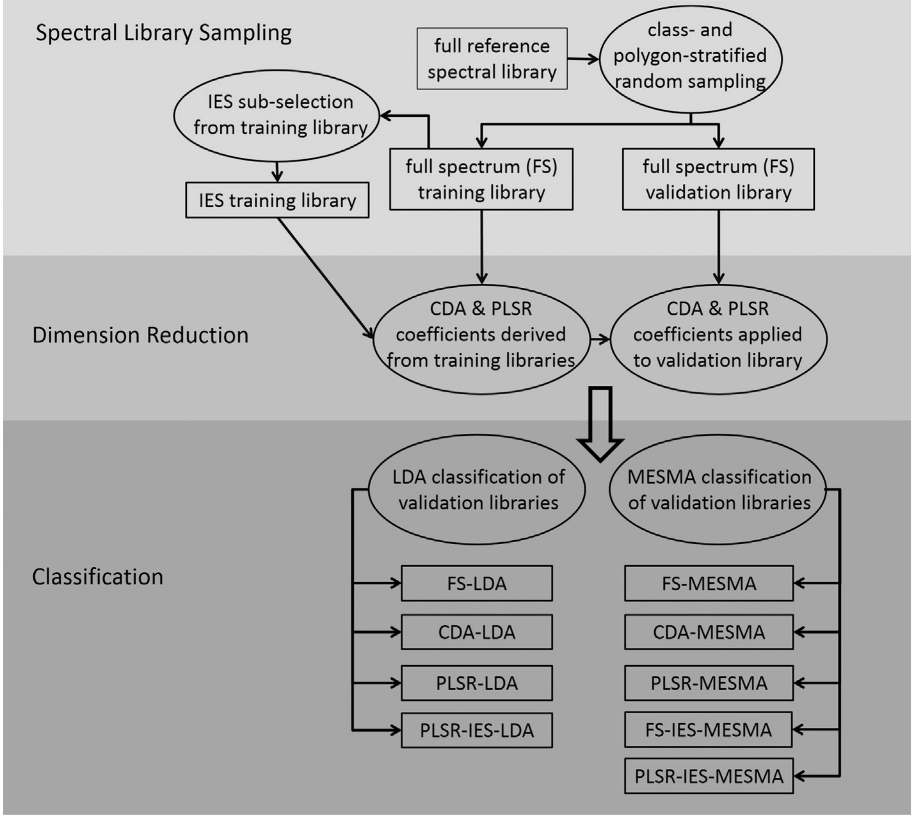

Fig. 2. Work flow diagram illustrating the classification processing steps for each study site from sampling the libraries into training and validation libraries, through dimension reduction and classification.

Please cite this article as: Roth, K.L., et al., Differentiating plant species within and across diverse ecosystems with imaging spectroscopy, *Remote Sensing of Environment* (2015), http://dx.doi.org/10.1016/j.rse.2015.05.007

for all sites simultaneously. The CS training library included 7657 spectra used to classify 121,399 validation spectra (a training sample proportion of about 6%). We classified the CS validation library using CDA dimension reduction with LDA, based on the single-site results.

3. Results

3.1. Spectral separability within individual ecosystems

Acceptable kappa values (>0.7) were achieved by at least one classification strategy for all sites but SNEV (Table 3). The highest mean kappa values across classification strategies were found for SERC, SFBR and Gulf sites (>0.8). Mean overall accuracy across strategies was greater than 75% for all sites except SNEV.

SERC had the second highest mean overall accuracy (86%) and the lowest standard deviation in kappa across strategies (0.03). Of 11 classes, the most well-discriminated were crop, soil and crop residue (mean producer's and user's accuracies $> 96\%$) (Fig. 3). Discrimination among the remaining dominant species varied, as can be seen in the wider range of accuracies for each species across the classification configurations (Fig. 3). The highest producer's and user's accuracies for the remaining eight species were achieved for *L. tulipifera* and *Fagus* spp. User's accuracies for all other tree species were low ($<50\%$). The most poorly discriminated classes included *Platanus occidentalis* and *Pinus* spp. Confusion among classes at SERC was the highest within the deciduous broadleaf tree PFT.

The Gulf site was the most accurately classified ecosystem, with a mean overall accuracy of 88% and a standard deviation in kappa across strategies of 0.06. Water classes were very accurately classified, having mean producer's and user's accuracies $>90\%$ (Fig. 4). However, species discrimination was also high. Of the 6 dominant plant species, 5 had average producer's accuracies $\geq 85\%$, and 4 had average user's accuracies $\geq 80\%$. The greatest confusion occurred between *J. roemerianus* and *Spartina alterniflora*.

WR had a mean overall accuracy of 78%, but kappa values >0.7 were only achieved by two classification strategies. The standard deviation in kappa was 0.05 for this site. Individual class accuracies at WR were generally very good, with 9 of 11 classes having average producer's accuracies $\geq 65\%$ and 8 classes with average user's accuracies $\geq 65\%$ (Fig. 5). Classes with both high producer's and user's accuracies included rock/soil and senesced grass, as well as *A. rubra*, *Acer macrophylla* and *P. menziesii*. Some classes had a high mean producer's accuracy, but low user's accuracy (e.g., *Pteridium aquilinum*, *Acer circinatum*). *Abies grandis* was the most poorly discriminated class, having an average producer's accuracy of 35% and an average user's accuracy of just 1%. At this site class confusion was the highest between the two dominant species: *P. menziesii* and *T. heterophylla*, though the mean class accuracies for both species were $\geq 69\%$

The SNEV site had the lowest overall accuracies (mean $= 55\%$), and the highest standard deviation of kappa among the sites (0.08). At SNEV, rock was the most easily discriminated class, followed by meadow (average producer's and user's accuracies $\geq 90\%$); each was well-classified by all configurations (Fig. 6). Producer's and user's accuracies varied greatly across classification configurations for the other species. Several methods produced reasonable producer's accuracies ($>60\%$) for some species including *Abies magnifica*, *Arctostaphylos* spp., *Ceanothus cordulatus*, *Salix* spp. and *Q. chrysolepsis*. However, the mean producer's accuracies across methods were less than 60% for most species. Classes that were poorly discriminated by all or most methods included *Calocedrus decurrens*, *Pinus jeffreyi*, *Pinus lambertiana* and *Sequoiadendron giganteum*. Confusion among classes was the highest among these needleleaf evergreen tree species.

SBFR was also well-classified by most methods, with a mean overall accuracy of 84% and a standard deviation of kappa of 0.04. The SBFR site was the most diverse of the five study regions, with 23 classes. Classifications at this site produced very good discrimination across species, with 18 classes having an average producer's accuracy and/or an average user's accuracy $>70\%$ across all configurations (Fig. 7). The classes with the highest average producer's accuracies included *Brassica nigra* (95%), marshes (96%), and *Eriogonum fasciculatum* (97%). Those with the highest average user's accuracies included *Eucalyptus* spp. and irrigated grasses (97%), as well as marsh wetlands and urban cover (98%). *P. sabiniana* was the only class with mean producer's accuracy below 60%, and *Baccharis pilularis* had the lowest mean user's accuracy (53%). Among classes, confusion was greatest between *A. fasciculatum* and *Arctostaphylos* spp., as well as between *P. sabiniana* and *Quercus douglasii*.

3.2. Classification strategy performance

Across sites and classification strategies, acceptable kappa values (>0.7) were achieved by all classification strategies for 3 of 5 sites (Table 3). The highest mean kappa values across sites were achieved by FS-LDA, CDA-LDA, and PLSR-MESMA. Overall accuracies averaged across sites were $\geq 74\%$ for all classification strategies. Repeated measures ANOVA of rank transformed overall accuracy and kappa values indicated that differences among the performance of configurations by site were significant at $p = 0.001$. However, the post-hoc multiple comparisons tests showed no significant differences among these six configurations.

Within each site, no single classification strategy far outperformed the others, and in most sites, the highest kappa was the same for two or more strategies. Likewise, overall performance differences among the strategies were similar for most sites. At SERC, all three LDA configurations produced the highest producer's and user's accuracies for most dominant plant species (Fig. 3). At the Gulf site, full spectrum LDA and PLSR-reduced MESMA yielded the highest kappa values, and differences

Table 3

Kappa values and overall accuracy summarized by site and classification configuration. Abbreviations are as follows: FS (full spectrum), CDA (CDA-reduced), PLSR (PLSR-reduced), LDA (linear discriminant analysis), and MESMA (multiple endmember spectral mixture analysis).

	SERC	GULF	WR	SNEV	SBFR	Config. mean kappa	Config. mean % overall accuracy
FS-LDA	0.85	0.90	0.75	0.56	0.84	0.78	82
CDA-LDA	0.85	0.87	0.75	0.56	0.84	0.77	81
PLSR-LDA	0.86	0.76	0.62	0.46	0.77	0.69	74
FS-MESMA	0.80	0.88	0.64	0.34	0.78	0.69	74
CDA-MESMA	0.79	0.80	0.69	0.50	0.87	0.73	78
PLSR-MESMA	0.80	0.90	0.69	0.49	0.87	0.75	80
Mean LDA kappa	0.85	0.85	0.7	0.52	0.82	0.75	79
Mean MESMA kappa	0.80	0.86	0.67	0.44	0.84	0.72	77
Mean FS kappa	0.82	0.89	0.69	0.44	0.81	0.73	78
Mean CDA kappa	0.82	0.84	0.72	0.53	0.86	0.75	79
Mean PLSR kappa	0.83	0.83	0.65	0.48	0.82	0.72	77
Site mean kappa	0.82	0.85	0.69	0.48	0.83		
Site mean % accuracy	86	88	78	55	84		

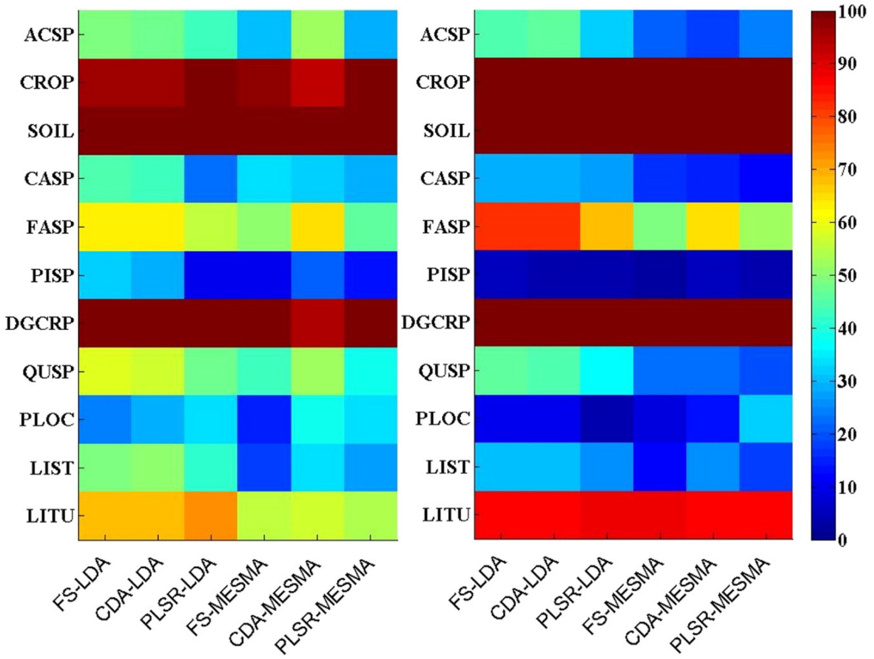

Fig. 3. Class-level producer's (left) and user's (right) accuracies for SERC. Classification configurations are listed along the X axis, and species and cover types are listed along the Y axis. The colors show % accuracy, from low (blue) to high (red). Abbreviations for classes can be found in Table 2, and abbreviations for configurations can be found in Table 3. (For interpretation of the references to color in this figure legend, the reader is referred to the web version of this article.)

in performance among classification configurations varied by class (Fig. 4). For some classes, such as *Spartina patens*, all configurations produced similar producer's accuracies, while for others, such as *J. roemerianus*, producer's accuracies ranged more widely. A similar pattern was observed with user's accuracies. Within the WR site, full-spectrum and CDA-reduced training libraries run with the LDA classifier were the best performing configurations (kappa = 0.75). Class-level accuracies varied across configurations, particularly for user's accuracies (Fig. 5). At SNEV, both full-spectrum and CDA-reduced full training library classifications with LDA again yielded the highest producer's accuracies across classes, and user's accuracies showed a similar pattern (Fig. 6). In contrast to the other sites, at SBFR, the two configurations with the highest average producer's and user's accuracies across species were CDA- and PLSR-reduced full training library MESMA (~87%) (Fig. 7). Classification configurations tended to produce similar results within a given class.

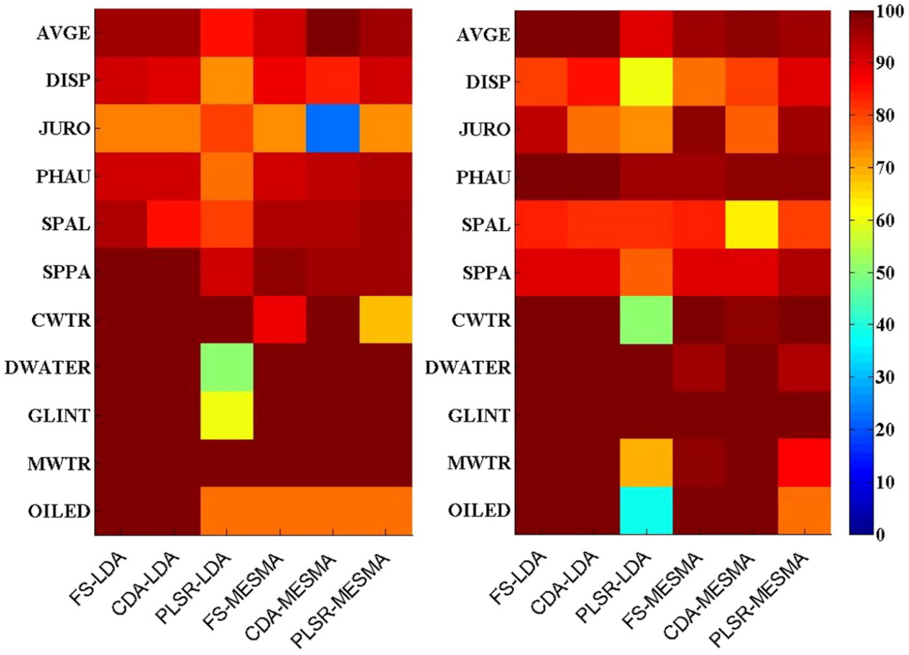

Fig. 4. Class-level producer's (left) and user's (right) accuracies for GULF. Classification configurations are listed along the X axis, and species and cover types are listed along the Y axis. The colors show % accuracy, from low (blue) to high (red). Abbreviations for classes can be found in Table 2, and abbreviations for configurations can be found in Table 3. (For interpretation of the references to color in this figure legend, the reader is referred to the web version of this article.)

Please cite this article as: Roth, K.L., et al., Differentiating plant species within and across diverse ecosystems with imaging spectroscopy, *Remote Sensing of Environment* (2015), http://dx.doi.org/10.1016/j.rse.2015.05.007

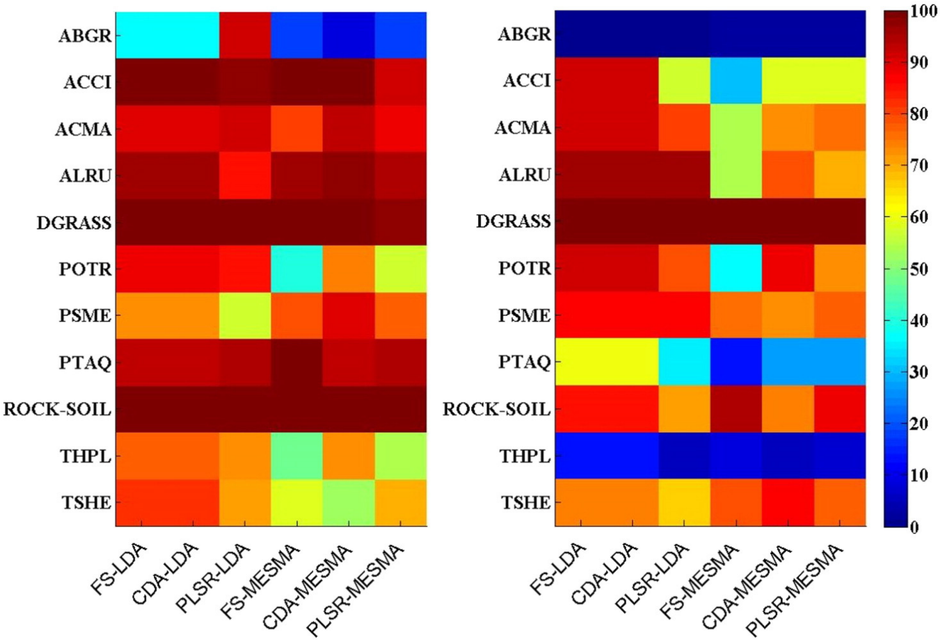

Fig. 5. Class-level producer's (left) and user's (right) accuracies for WR. Classification configurations are listed along the X axis, and species and cover types are listed along the Y axis. The colors show % accuracy, from low (blue) to high (red). Abbreviations for classes can be found in Table 2, and abbreviations for configurations can be found in Table 3. (For interpretation of the references to color in this figure legend, the reader is referred to the web version of this article.)

3.2.1. Dimension reduction

Using full-spectrum or dimension-reduced data affected classification accuracy, as did choice of reduction method (Table 3). Considering both classifiers, kappa values for configurations using CDA dimension reduction were higher than those using full-spectrum data for SNEV, SBFR and WR, similar for SERC, and lower for the Gulf site. However, when LDA was the classifier, full-spectrum and CDA-reduced accuracies were nearly identical for all sites except the Gulf. Dimension reduction with PLSR resulted in higher accuracies than full-spectrum data at all sites when MESMA was used as the classifier and lower accuracies at all sites but SERC when LDA was the classifier. In general, configurations using MESMA yielded higher accuracies when used with dimension reduction, and CDA- and PLSR-reduced libraries performed similarly for all sites but the Gulf. These results are further supported by patterns observed in the individual class accuracies (Figs. 3–7). With the exception of SERC, configurations using either full-spectrum or CDA-reduced data

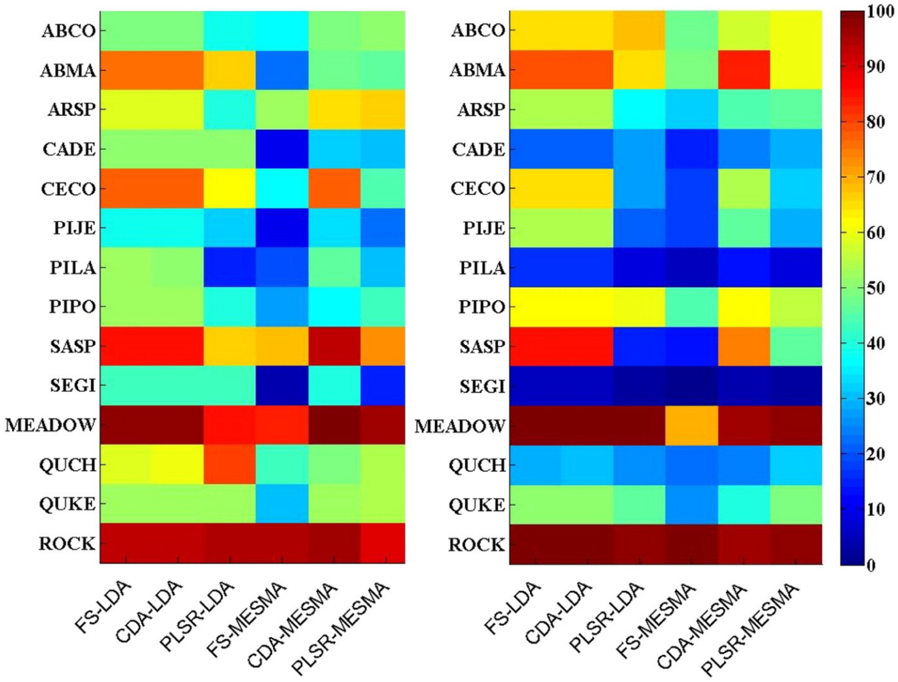

Fig. 6. Class-level producer's (left) and user's (right) accuracies for SNEV. Classification configurations are listed along the X axis, and species and cover types are listed along the Y axis. The colors show % accuracy, from low (blue) to high (red). Abbreviations for classes can be found in Table 2, and abbreviations for configurations can be found in Table 3. (For interpretation of the references to color in this figure legend, the reader is referred to the web version of this article.)

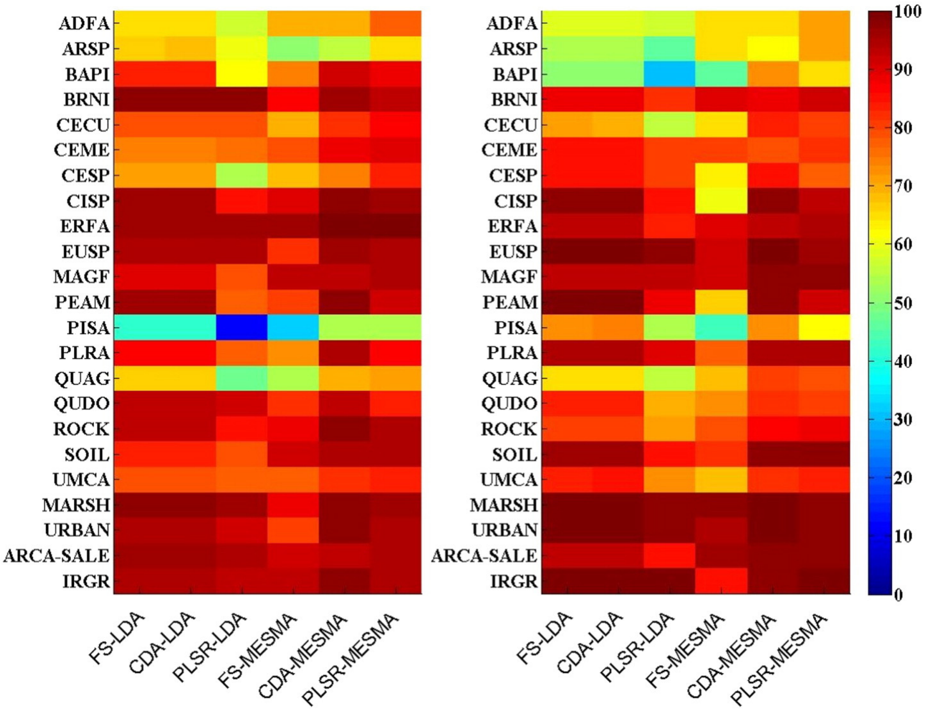

Fig. 7. Class-level producer's (left) and user's (right) accuracies for SBFR. Classification configurations are listed along the X axis, and species and cover types are listed along the Y axis. The colors show % accuracy, from low (blue) to high (red). Abbreviations for classes can be found in Table 2, and abbreviations for configurations can be found in Table 3. (For interpretation of the references to color in this figure legend, the reader is referred to the web version of this article.)

had the highest mean kappa values within individual sites (Table 3). When averaged across both configurations and sites, dimension reduction with CDA yielded the highest mean kappa (Table 3) as compared with full-spectrum and PLSR-reduced configurations.

3.2.2. Classifier

Generally, configurations using LDA as the classifier yielded similar or higher mean site kappa values than did those using MEMSA (Table 3). For configurations that used the full-spectrum training libraries, LDA achieved an average overall accuracy 7.8 percentage points (pp) higher than MESMA. When the training libraries were CDA-reduced, LDA outperformed MESMA by just 3.6%. However, when these same libraries were PLSR-reduced, MESMA yielded higher accuracies all sites except SERC, achieving an average overall accuracy 5.4 pp higher than LDA.

Classifier performance within individual sites varied by configuration. At SERC, both MESMA and LDA were able to discriminate spectrally unique classes such as rock, crop, and crop residue from the remaining species with high levels of accuracy, but LDA was more accurate than MESMA when discriminating among the major deciduous tree species, though these accuracies were not very high in general (Fig. 3). In the Gulf site, LDA and MESMA classifications produced comparable accuracies overall, but MESMA yielded higher producer's and user's accuracies for 7 and 6 classes, respectively (Fig. 4). At WR, LDA achieved much higher producer's accuracies for some classes, notably *A. grandis*, *P. trichocarpa* and *T. heterophylla* and higher user's accuracies for the majority of classes (Fig. 5). At WR, both techniques fairly accurately classified meadow, *Salix* spp. and rock, but LDA was better able to distinguish among the pine and fir species in the classification (Fig. 6). Across all classes, LDA classifications outperformed MESMA in both producer's and user's accuracies by 11 pp and 8 pp on average. The SBFR site was the only site at which MESMA more frequently outperformed LDA. The greatest increases in class-level producer's and user's accuracies were observed when spectra were dimension reduced with either CDA or PLSR (Fig. 7).

3.3. Combined-ecosystem classification

We calculated the mean rank across all four performance metrics to determine the final rank for each configuration (Table 4). The resulting performance ranking indicated that LDA with a full-spectrum training library was the best strategy among those tested for classifying dominant species and cover types. This approach was nearly tied by LDA used with a CDA-reduced training library. We elected to use the latter strategy for the combined sites analysis because dimension reduction improves computational efficiency and increases interpretability, both of which will be important when mapping species at regional scales. Before applying this approach to the full CS library, we created dominant species maps at each of the sites to evaluate its performance on entire scenes. Figs. 8 and 9 show portions of these maps created for the SBFR and WR sites. In each site map, we observed the expected spatial distributions of dominant species. At SBFR, we are able to see the dominance of herbaceous species and sage scrub at lower elevations interspersed with citrus and avocado orchards. At higher elevations, the chaparral species become dominant. Riparian zones are dominated by *Quercus*

Table 4
Performance metrics and ranking for comparing classification configurations. PA is producer's accuracy and UA is user's accuracy.

	Mean % classes with PA & UA >= 60%	Mean % classes PA top performer	Mean % classes UA top performer	Mean kappa	Final rank
FS-TR-LDA	69	54	73	0.78	1
CDA-TR-LDA	69	50	72	0.77	2
CDA-TR-MESMA	59	54	40	0.73	3
PLSR-TR-MESMA	58	37	37	0.75	4
PLSR-TR-LDA	51	27	27	0.69	5
FS-TR-MESMA	49	22	28	0.69	6

Please cite this article as: Roth, K.L., et al., Differentiating plant species within and across diverse ecosystems with imaging spectroscopy, *Remote Sensing of Environment* (2015), http://dx.doi.org/10.1016/j.rse.2015.05.007

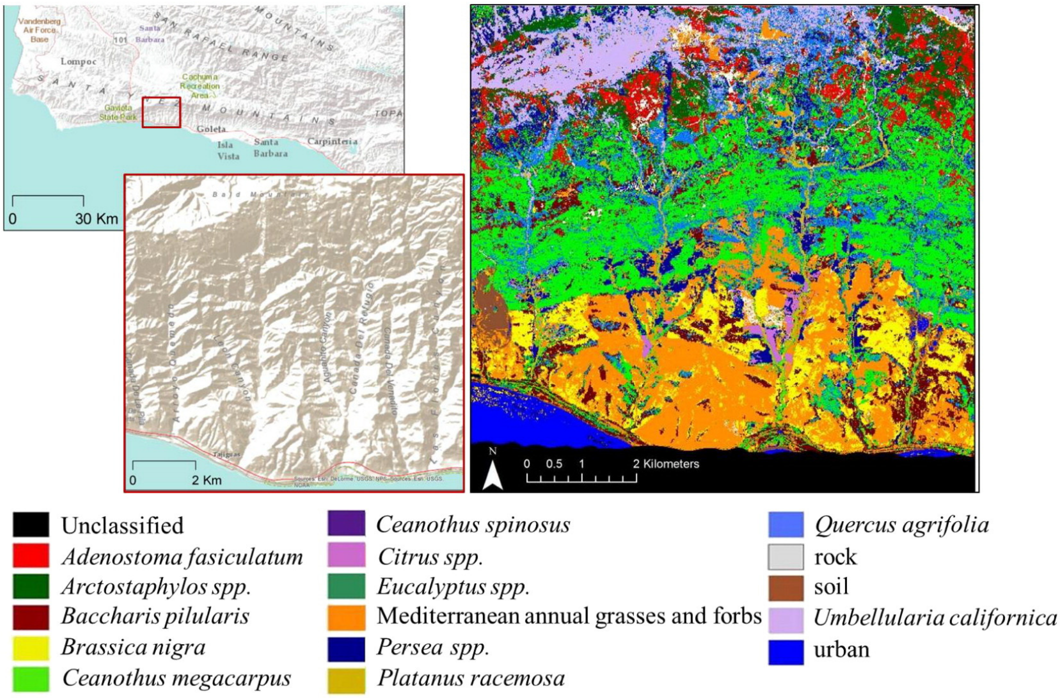

Fig. 8. Excerpt from the dominant species and land cover map at the Santa Barbara (SBFR) site generated using CDA-reduced spectra classified with Linear Discriminant Analysis (CDA-LDA) at 12 m spatial resolution and overall accuracy = 85%.

agrifolia, *U. californica* and *P. racemosa*. Within the WR map, we see the greatest coverage by the two most dominant species, *P. menziesii* and *T. heterophylla*. Forest gaps contain senesced grass, bracken fern (*P. aquilinum*) and vine maple (*A. circinatum*). Broadleaf deciduous species, such as *P. trichocarpa*, *A. rubra* and *A. macrophylla* are found in moister areas near the river.

Using CDA dimension reduction and LDA as the classifier with just a 6% training sample, we achieved an overall classification accuracy of 70%

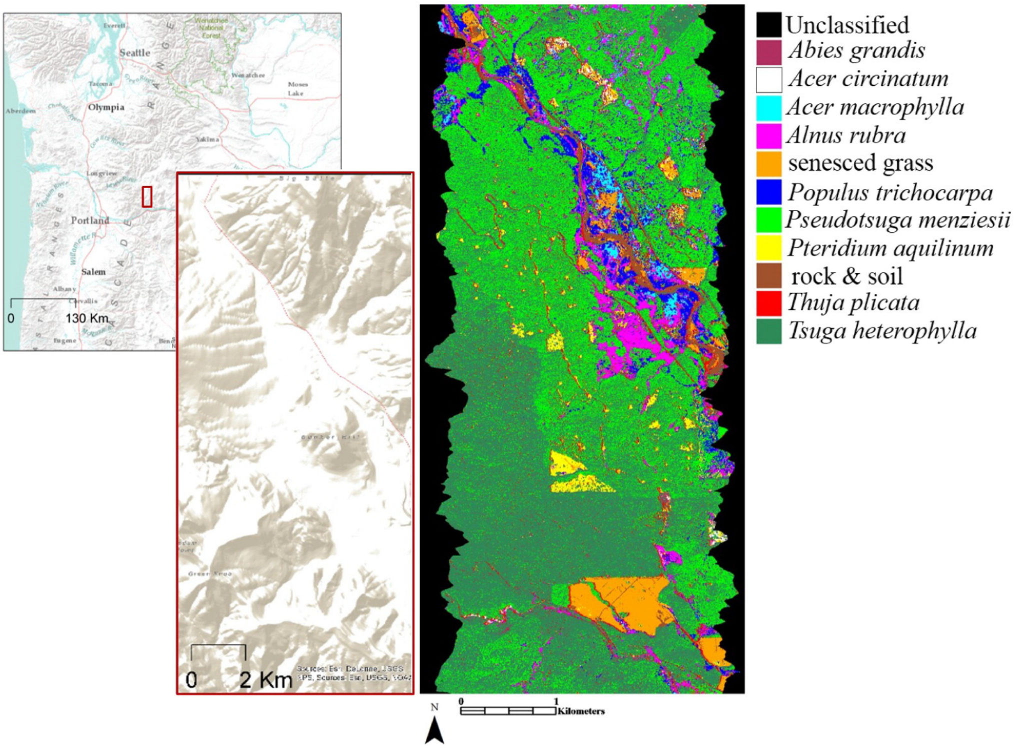

Fig. 9. Excerpt from the dominant species and land cover map at the Wind River (WR) site generated using CDA-reduced spectra classified with Linear Discriminant Analysis (CDA-LDA) at 4 m spatial resolution and overall accuracy = 82%.

Table 5

Combined-site classification results with producer's (PA) and user's (UA) % accuracies. For each class, the “Classified As” column contains the name of the class it was most frequently erroneously mapped as, and the “Classified” column contains the name of the class it most frequently erroneously mapped, based on the error matrix. Notations: ^{p} same PFT or cover type; ^{g} same genus; ^{c} co-occurring/intermixed; ^{i} infrequent (<0.05% of library); ^{f} frequent (>5% of library).

PFT	Site	Species or cover	PA	Classified As	UA	Classified
Annual herbaceous	SBFR	IRGR	93	MAGF^{p,g}	100	n/a
	SERC	CROP	98	PISP	100	n/a
	SNEV	MEADOW	96	CECO	100	ABMA
Deciduous broadleaf shrub	WR	ACCI ^{i}	100	n/a	73	ACMA^{c}, PSME^{c}
Deciduous broadleaf tree	SBFR	PLRA	84	QUAG^{c}	95	URBAN^{c}
		QUDO	92	ERFA^{c}	80	PISA^{c}
	SERC	ACSP	45	LIST^{p,c}	42	LITU^{p,c}
		CASP	38	LITU^{p,c}	44	LITU^{p,c}
		FASP	62	QUSP^{p,c}	77	ACSP^{p,c}
		LITU	76	PISP^{c}	90	CASP^{p,c}
		LIST	49	LITU^{p,c}	30	LITU^{p,c}
		PLOC	14	LIST^{p,c}, ACSP^{p,c}	5	LITU^{p,c}, LIST^{p,c}
		QUSP	51	LITU^{p,c}	45	FASP^{p,c}
	SNEV	QUKE	55	QUCH^{g,c}	39	ABCO
		SASP	90	CECO	36	QUKE^{p},^{c}
	WR	ACMA	86	POTR^{p,c}	89	POTR^{p,c}
		ALRU	93	POTR^{p}	97	POTR^{p}
		POTR	87	THPL	84	ALRU^{p}
Drought-deciduous shrub	SBFR	ARCA-SALE	96	BAPI^{c}	88	ERFA^{p}
Evergreen broadleaf shrub	GULF	AVGE	84	SPAL	99	DISP, PHAU
	SBFR	BAPI	71	ARCA-SALE^{c}	42	MAGF^{c}
		CECO	84	ABCO^{c}	40	PIPO^{c}
		CECU	79	ERFA^{c}	63	PISA^{c}
		CEME	79	ADFA^{c}	82	CESP^{g,p,c}
		CESP	67	CEME^{g,p,c}	80	PLRA
	SBFR, SNEV	ARSP	13	ADFA^{c}, QUCH^{c}	53	ROCK_SOIL^{c}
Evergreen broadleaf tree	SBFR	CISP	97	URBAN^{p,c}	96	PEAM^{p}
		EUSP	95	MAGF^{c}	99	BAPI, MARSH, PLRA, URBAN^{c}
		PEAM	94	QUAG^{p}	100	n/a
		QUAG	64	BAPI	63	PLRA^{c}
		UMCA	79	QUAG^{p,c}	84	QUAG^{p,c}
	SNEV	QUCH	60	QUKE^{g,c}	18	ARSP^{c}, QUKE^{g,c}
Evergreen needleleaf shrub	SBFR	ADFA	89	ARSP^{c}	46	ARSP^{c}
		ERFA	96	ARCA-SALE^{p}	89	CECU^{c}
Evergreen needleleaf tree	SBFR	PISA	24	QUDO^{c}	66	QUAG^{c}
	SERC	PISP	26	LISP^{c}, LQSP^{c}	4	LISP^{c}, CROP
	SNEV	ABCO^{f}	52	PIPO^{p,c}	59	PIPO^{p,c}
		ABMA	81	SEGI^{p,c}	75	ABCO^{g,p,c}
		CADE	36	ABCO^{p,c}	21	ABCO^{p,c}, PIPO^{p,c}
		PIJE	29	PIPO^{g,p}	40	PIPO^{g,p}
		PILA	17	CADE^{p,c}	7	ABCO^{p,c}, PIPO^{g,p,c}
		PIPO^{f}	39	ABCO^{p,c}	56	ABCO^{p,c}
		SEGI	52	ABMA^{p,c}	3	ABCO^{p,c}, ABMA^{p,c}
	WR	ABGR^{i}	55	THPL^{p}	0	PSME^{p}, TSHE^{p}
		PSME^{f}	60	TSHE^{p,c}	92	TSHE^{p,c}
		THPL	72	ABGR^{p}	5	PSME^{p}, TSHE^{p}
		TSHE^{f}	80	ABGR^{p}	68	PSME^{p,c}
Perennial herbaceous	GULF	DISP	72	SPPA^{p}	51	PHAU^{p}
		JURO	54	SPAL^{p}	74	SPAL^{p}
		PHAU	70	DISP^{p}	93	SPPA^{p}
		SPAL	88	JURO^{p}	69	JURO^{p}
		SPPA	83	DISP^{p}	74	PHAU^{p}
	SBFR	MARSH	97	BAPI	98	URBAN
	WR	PTAQ	90	POTR	49	PSME
Senesced annual herbaceous	SBFR	MAGF	86	BRNI^{p,c}	94	ROCK_SOIL^{c}
		BRNI	97	BAPI^{c}	85	MAGF^{p,c}
	SERC	DGRCRP	100	n/a	100	n/a
	WR	DGRASS	99	ABGR	100	n/a
Senesced vegetation	GULF	OILED^{i}	75	BRNI^{p}	33	ROCK_SOIL^{c}
n/a	All	ROCK_SOIL	90	ARSP^{c}	97	MAGF
	GULF	CWTR^{i}	100	n/a	100	n/a
		DWATER	100	n/a	100	n/a
		GLINT	60	MWTR	97	URBAN^{p}
		MWTR	100	n/a	68	GLINT
	SBFR	URBAN	92	BAPI	99	ROCK_SOIL^{p}

for the combined-site validation library. Of the 65 classes included in the analysis, well over half had producer's or user's accuracies ≥70% (41 and 35, respectively) (Table 5). Furthermore, 22 classes had a producer's accuracy ≥90%, as did 20 classes for user's accuracy. The most accurately discriminated classes covered nearly the entire range of PFTs and cover types, including annual herbaceous species (e.g., crop, meadow), deciduous broadleaf and drought-deciduous shrubs, several broadleaf deciduous and evergreen trees, most evergreen broadleaf and needleleaf

Please cite this article as: Roth, K.L., et al., Differentiating plant species within and across diverse ecosystems with imaging spectroscopy, *Remote Sensing of Environment* (2015), http://dx.doi.org/10.1016/j.rse.2015.05.007

shrubs, a few perennial herbaceous species, senesced vegetation and other cover types (e.g., water, rock, urban). The lowest accuracies were among several of the broadleaf deciduous tree species (mainly from SERC) and among needleleaf evergreen tree species (at most sites).

Mean site-level producer's and user's accuracies decreased slightly (by 2–14 pp and 0–16 pp, respectively), from single site to combined-site classification, with the largest decrease for the Gulf site classes. Individual class-level accuracies remained similar (+/−3 pp) to those of the single-site classifications for approximately half the classes, and those with changes >3 pp were roughly evenly distributed among all sites. Accuracies decreased by 10 pp or more for 17 (producer's) and 13 (user's) classes, and increased by 10 pp or more for just 3 classes. Confusion among classes followed similar patterns to single site classifications (Table 5). Although the most frequently confused classes were often within the same ecosystem, there were also cases of confusion among classes from different ecosystems. These nearly always occurred within PFTs. For example, confusion occurred between two evergreen needleleaf trees, *C. decurrens* (SNEV) and *A. grandis* (WR). Similarly, senesced vegetation from the Gulf site was erroneously classified as *B. nigra* (SBFR), likely because, in addition to being senesced, both classes have greater vertical structure than grasses and forbs

4. Discussion

4.1. Spectral separability of dominant species

Our ability to spectral separate dominant species and cover types within each ecosystem using imaging spectroscopy data was driven by three factors: 1) the diversity and distinctiveness of PFTs present, 2) the spectral similarity of species within the same PFT, and 3) the abundance and spatial distribution of species within the landscape. At all sites, spectrally unique cover types, such as rock or soil, were accurately mapped. Among vegetation classes, the most common sources of error were confusion among species within the same genus or PFT and confusion among species which grow in mixed stands or patches.

Conventional PFTs capture several of the major biological differences among species in an ecosystem that influence their spectral signatures (e.g., deciduous vs. conifer) (Plourde et al., 2007; Van Aardt & Wynne, 2001). Differences in some characteristics, like life form, result in greater spectral differences than others, making a PFT more distinct. Likewise, shared characteristics between PFTs may result in greater spectral similarity. Our results from the SNEV, WR and SERC ecosystems illustrate this point. These three sites have the same number of PFTs, but overall accuracies were high at SERC, moderate at WR and low at SNEV. The high overall accuracies observed at SERC were driven by the set of very distinct PFTs found in this ecosystem. At WR, accuracy was bolstered by the contrast between evergreen needleleaf and deciduous broadleaf trees, as well as by the presence of both live and senesced herbaceous PFTs. The PFTs at SNEV are more similar than those at found at WR and SERC, particularly species distributed among 3 tree PFTs.

Within a PFT, species may have additional characteristics that make them spectrally distinct, but likely spectral signatures are more similar. At SERC, SNEV and WR, half or more of the species fall into a single PFT for which class-level accuracies are lower and confusion among species is high. Even so, the Gulf was one of the most accurately classified sites despite having the lowest PFT diversity and the majority of plant species in a single PFT. The high spectral separability among species in this site is most likely due to the structural differences in both leaf shape and plant form (Zomer, Trabucco, & Ustin, 2009) or phenological differences (Ouyang et al., 2013). At the other end of the continuum, the SBFR site had the highest PFT diversity (9), with each PFT having between 1 and 5 species, and was also very accurately classified. These results are particularly encouraging given the sheer number of vegetation classes (20). Confusion within PFTs was also observed here, but was quite low compared to the other sites. Similarly high accuracies have been previously reported for this site, and the number and diversity of vegetation classes included in our study is even greater (Dennison & Roberts, 2003a; Roth et al., 2012).

Thought we can spectrally differentiate more specific classes than just conventional PFTs, there may be limitations to how well species within these PFTs (e.g., evergreen needleleaf trees) can be separated. The unique plant types that can be detected using optical remote sensing data are called ‘optical PFTs’, which characterize vegetation by differences in structure, biochemistry, physiology and phenology (Ustin & Gamon, 2010). While single date imaging spectroscopy data capture some of these differences, more explicit incorporation of structure (e.g., from lidar) and/or phenology could improve our ability to differentiate among plant species. Indeed studies have found the use of structural information (Alonzo, Bookhagen, & Roberts, 2014; Colgan, Baldeck, Féret, & Asner, 2012; Dalponte, Bruzzone, & Gianelle, 2012) and phenological information (Hunt & Williams, 2006; Somers & Asner, 2012) with imaging spectroscopy data does improves species discrimination. HyspIRI would provide monthly images, making multi-temporal analyses possible, and while coincident lidar and imaging spectroscopy data sets have been few in the past, the establishment of the National Ecological Observation Network and its Airborne Observation Platform (AOP) (Kampe et al., 2010) mean these types of datasets will be acquired over a diversity of ecosystems in the coming years. Higher spectral resolution or the incorporation of spatial information from fine resolution imagery, collected by aerial sensors like AVIRIS Next Generation, may also be able to better highlight key spectral differences needed to tell species apart (Van Aardt & Wynne, 2007).

The third major control on the spectral separability of species in each ecosystem was their abundance and spatial distribution within the landscape. Species that occur less frequently in the landscape, or occur only within small patches, were difficult to classify accurately (similar to findings by Waser & Asner, 2011). For example, *C. cordulatus*, a shrub at the SNEV site with very low accuracies, occurs mainly in small, isolated patches within the greater matrix of fir and pine trees, and at WR the lowest class-level accuracies occurred due to confusion between two infrequent classes (*A. grandis* and *Thuja plicata*). Similar results were reported for *A. grandis* by Jones, Coops, and Sharma (2010). Classes such as these were difficult to separate accurately for two primary reasons. First, a small training data set limits our ability to establish what makes this species spectrally distinct from others, and second, there is a greater likelihood of training data where a pixel contains >1 dominant species. This second point is perhaps the most important for understanding the majority of class confusion within ecosystems and the impact on overall accuracies.

In many ecosystems, two or more species may be co-dominant, or grow intermixed in the landscape. In these cases, reference patches, such as those collected for this study, are likely to contain some pixels dominated by another species or, if the species are mixed homogenously within the patch, most pixels will contain both species. This can lead to two types of error in mapping that result in lower accuracy and higher confusion between the species. In the first case, the classification may accurately classify a pixel, but because this pixel belongs to a reference patch of another species, it will incorrectly be called an error. In the second case, the training spectral signatures will also be mixed, causing the two species look similar even if their pure signatures are separable. There are several examples from our study that illustrate these points. At SBFR, *A. fasciculatum* and *Arctostaphylos* spp. occur most frequently in co-dominated patches ranging from 60/40 to 40/60. Here it is likely that many correctly classified pixels are calculated as errors. At the SNEV, *C. decurrens*, *P. ponderosa* and *P. lambertiana* all grow very highly intermixed, making establishing unique training signatures for each species quite challenging and resulting in high levels of confusion among these classes. Similar patterns were observed at the SERC, SBFR and Gulf sites. Building reliable and spatially extensive reference data sets is a major challenge for species' mapping, and there are tradeoffs in collecting

Please cite this article as: Roth, K.L., et al., Differentiating plant species within and across diverse ecosystems with imaging spectroscopy, *Remote Sensing of Environment* (2015), http://dx.doi.org/10.1016/j.rse.2015.05.007

these data that must be taken into account, particularly when using the resulting maps.

Given the role class abundance and distribution play in spectral separability, the spatial resolution of the images used becomes a key factor. The image data for the sites with the lowest accuracies (SNEV and WR) were acquired at the finest spatial resolution (3.3 & 3.5 m, respectively). On one hand, this may have resulted in fewer pixels containing >1 species, and on the other, the highly mixed distribution of conifer species across the landscape means that reference polygons (>70% coverage by the dominant) almost certainly contained pixels that were purely another species. Furthermore, the open canopy architecture of these two conifer-dominated ecosystems means that finer spatial resolution data likely result in much higher within-class spectral variance. For example, despite having a similar spatial resolution (4 m), the classification accuracies for broadleaf-dominated SERC were much higher, perhaps due in part to a closed canopy with fewer shadows. Lastly, the drivers of species' spectrally separability may change with changing image resolution. For example, slightly coarser spatial resolutions could potentially reduce within canopy spectral variance, improving the training signatures for species with more open or non-uniform canopies. While these differences were not examined in depth in this study, they will be considered in subsequent work.

4.2. Selecting a classification strategy

Our results in comparing different strategies demonstrate there is not a one-size-fits-all answer for classifying dominant species across diverse ecosystems. Although dimension reduction is often used when working with hyperspectral data, our findings did not show statistically significant improvements to overall classification accuracy with either CDA or PLSR. That said, given a sharp increase in computational efficiency when using fewer bands, and neutral effect on accuracy, dimension reduction makes sense. CDA-reduced LDA classifications produced nearly equivalent kappa values across sites, which is not surprising, given that CDA is a variant of LDA (Zhao & Maclean, 2000). Although few studies have applied a dimension reduction transform when using MESMA for classification (see Li et al., 2005), dimension reduction should lead to fewer classification errors simply because the bands that contribute more to discrimination are more heavily weighted by the coefficients. Findings by Somers and Asner (2013) demonstrate this concept, using multi-temporal data to improve MESMA classification of native and invasive Hawaiian species. In the current study, dimension reduction with CDA led to mixed changes in accuracy by ecosystem. By contrast, using PLSR improved MESMA classification results at all five sites. It is interesting to note that MESMA achieves the best results with PLSR dimension reduction while LDA achieves the best results using CDA dimension reduction. The formulation of each technique may explain this observation. Evaluating the mathematical relationship between dimension reduction techniques and classifiers may aid scientists in identifying pairs that work best together.

Both classifiers used in this study were able to accurately differentiate dominant species. These findings support those of other studies which have used LDA or MESMA for species classification (Féret & Asner, 2012b; Roth et al., 2012; Somers & Asner, 2013; Suzuki, Okamoto, Takahashi, Kataoka, & Shibata, 2012). Our results show that, when using the full spectrum, LDA yields higher accuracies than does MESMA in the majority of ecosystems assessed here. In particular, while both techniques are able to accurately differentiate spectrally unique classes, such as rock or soil, LDA is better able to separate spectrally similar classes, such as the broadleaf deciduous tree species at SERC or the pine and fir species at SNEV. This indicates that if only subtle spectral differences exist for a class, LDA can give these differences higher weight in the classification. MESMA, on the other hand, is based on overall fit and has no a priori class knowledge. Therefore it is not able to highlight key differences for very spectrally similar classes. Indeed, MESMA performed better when used with a dimension reduction technique that does incorporate this a priori class knowledge. This finding could bolster the utility of MESMA as a classification technique. Furthermore, most reference datasets will not include an exhaustive list of the dominant species found over these large regions. The presence of an 'unclassified' option for assigning a pixel to a class is important in this context. LDA does not have this option, nor is there a relatively straightforward way to implement it by, for example, thresholding a pixel's discriminant score. With MESMA, a user is able to specify an RMSE threshold, and, if no training spectrum fits a pixel well, this pixel will be labeled 'unclassified.'

Though we did not explicitly consider uncertainty estimates in this study, this is an important consideration in classification (Rocchini et al., 2013). Maps of spatial uncertainty provide critical information to map users and can provide insights to the limitations of a method (Kyriakidis & Dungan, 2001). It is important to note that different types of uncertainty exist in a classification analysis, and caution must be used when comparing different metrics for different classification algorithms. One approach for MESMA is to calculate and map the pixels in an image classified by very accurate endmembers. For example, Youngentob et al. (2011) created maps showing pixels modeled by MESMA endmembers with ≥75% accuracy for classifications of two eucalypt species. Likewise, extensions to LDA have been proposed and tested, such as Robust Fisher's Discriminant Analysis, which directly incorporate measures of class uncertainty (Kim et al., 2005).

4.3. Relevance to HyspIRI

Our combined ecosystems analysis evaluated the potential for mapping dominant plant species and cover types using with imaging spectroscopy data simultaneously across multiple ecosystems, as would be possible using HyspIRI. We were able to discriminate among dominant species with fairly high overall accuracy (70%), and with good class-level producer's and user's accuracies for most classes. With much higher diversity in the classification, many class-level accuracies decreased relative to the single-site classifications, user's accuracies in particular. This may be a concern if multiple-ecosystem classification maps are generated. We also observed a greater impact on accuracy with decreasing class size. Infrequent classes (<0.05% of the full library or about 50 spectra) that were spectrally unique had reasonably high accuracies. However, small classes with inter-mixing and functionally similar co-dominants had the lowest accuracies. Only a minor amount of confusion within PFTs was observed between species from different ecosystems, and species that occurred in multiple ecosystems were accurately classified. We also found that the correct species were mapped to each ecosystem, raising the question of how spectrally unique ecosystems are from one another, given their PFT and species composition.

Collecting quality species' reference spectra to be used with HyspIRI imagery and ensuring these training spectra are representative of their class is no small task. Our results demonstrate high accuracies can be achieved using only a small proportion of the reference data for training. However, as large spectral library databases are created in support of spaceborne hyperspectral missions, reliable protocols for selecting suitable reference spectra and evaluating the usefulness of these spectra will be necessary. Although the IES algorithm did not perform well in this study, its performance may improve if applied to the entire reference spectral library, rather than the training library. Subsequent improvements to the IES algorithm code have enabled this option for future research (Dudley, Dennison, Roth, Roberts, & Coates, in press). In cases where little training data are available strategies without a minimum sample requirement (e.g., PLSR dimension reduction or MESMA) may be needed. Though it should be noted that, in our study, kappa values for PLSR-reduced MESMA were much lower when using the IES-selected training library. This demonstrates that, while a minimum sample size may not be necessary to use some methods, there may be a minimum sample size necessary to accurately map dominant species

When mapping dominant species in a single ecosystem, computational efficiency may not be a major factor. However, as we move to mapping species over larger regions, it becomes a critical consideration for choosing a classification approach. Using dimension reduction improves computational efficiency, as does selecting a smaller training data set (with a technique such as IES). This is particularly important for iterative classifiers, like MESMA, where classification could become a lengthy process if thousands of full-spectrum spectra are being fitted to each pixel over large regions of Earth's surface.

Understanding the effects of spatial, spectral and temporal resolution on our ability to discriminate species within and across ecosystems is an active area of research, and one that will benefit immensely from a global spaceborne mission. In this line, we are not simply trying to create the most accurate map, but also to better understand *why* we are able to spectrally separate classes, exploring which parts of the spectrum contribute most to the discrimination and using this to improve our understanding of species' differences across space and time. This comprehension invariably leads to improved strategies for classification. Of the strategies evaluated in this study, only full-spectrum LDA does not allow for interpretation (Klecka, 1980). With MESMA each classified pixel can be tied to one spectrum in the reference library (the best fit). Additionally, the coefficients generated by both CDA and PLSR are interpretable, though each method's coefficients represent different information. In fact, these two techniques may produce even better discrimination results if combined. Canonical Partial Least Squares (CPLS), proposed by Indahl, Liland, and Naes (2009) incorporates the strengths of both PLS and canonical correlation analysis (CCA; closely related to CDA) and aims to incorporate more discriminatory information in fewer components to achieve higher accuracies.

5. Conclusions

Mapping dominant plant species over a wide range of ecosystems will provide critical information for addressing ecological questions about species' distributions, disturbance, climate change and ecosystem function. Imaging spectroscopy data is extremely well-suited for this purpose, and the launch of a spaceborne imaging spectrometer, like HyspIRI, will make these data available on a scale much larger than ever before. Our study demonstrates that we can successfully discriminate dominant plant species and cover types from five diverse ecosystems containing 58 unique vegetation classes distributed over a wide geographic area. Species from one region were not confused with another, suggesting that a global mission can map plant species over large geographic regions, a promising result for a sensor like HyspIRI. Furthermore, this was accomplished using image data collected over a wide range of illumination and viewing geometries and atmospheric conditions.

Dominant species' separability within a given ecosystem was mainly related to the diversity and distinctiveness of the PFTs present, the spectral similarity among species within each PFT, and the distribution of species across the landscape. Species' spectral differences are likely expressions of functional differences (Ustin & Gamon, 2010), and the magnitude and seasonal timing of these differences have important ramifications for our ability to discriminate among species within similar functional classes. The impact of dominant species' occurrence and spatial distributions within ecosystems on mapping accuracy is also an important consideration, especially when scaling these results to the proposed resolution of spaceborne imaging spectrometer missions (30–60 m).

Of the classification strategies evaluated, none was clearly the best in every ecosystem. However, three showed considerable promise — using the full spectrum training spectra and LDA, CDA for dimension reduction with LDA, and PLSR dimension with MESMA. The use of dimension reduction resulted in the same or higher accuracy as compared to the full spectrum data and has three major advantages for broad scale species mapping: increased computation efficiency, a reduced number of training samples required and greater interpretability of the classification process. While our results were achieved using finer spatial resolution than will be acquired with HyspIRI, subsequent research will address this question. Furthermore, a spaceborne mission will have advantages resulting from repeat sampling (including the possible incorporation of phenological information) and more favorable lighting geometry.

Acknowledgments

We would like to thank all those who contributed to field data collection for this research, especially Geoffrey Parker, Gregory Fryer, Michael Toomey and Bree Belyea. Thanks to NASA JPL AVIRIS team for collecting and providing the image data. Funding for this study was provided by NASA grants NNX12AP08G, HyspIRI discrimination of plant species and functional types along a strong environmental-temperature gradient and NNX08AM89G, Spatial, Spectral and Temporal Requirements for Improved Hyperspectral Mapping of Plant Functional Types, Plant Species, Canopy Biophysics and Canopy Biochemistry, and in part by a proposal to the NSF Rapid Grant Program entitled "Analysis of NASA's Advanced Visible Infrared Imaging Spectrometer Data Acquired Over Multiple Dates and Flight lines along the Northern Gulf Coastline, including Barrier Islands," (Principal Investigator S. Ustin). We would also like to thank the two anonymous reviewers for their valuable input and recommendations and the editor for his guidance in improving this work.

References

Alonzo, M., Bookhagen, B., & Roberts, D. A. (2014). Urban tree species mapping using hyperspectral and lidar data fusion. *Remote Sensing of Environment*, *148*, 70–83. http://dx.doi.org/10.1016/j.rse.2014.03.018.

Alonzo, M., Roth, K., & Roberts, D.A. (2013). Identifying Santa Barbara's urban tree species from AVIRIS imagery using canonical discriminant analysis. *Remote Sensing Letters*, *4*(5), 513–521.

Asner, G. (1998). Biophysical and biochemical sources of variability in canopy reflectance. *Remote Sensing of Environment*, *64*(3), 234–253.

Asner, G.P. (2013). Biological diversity mapping comes of age. *Remote Sensing*, *5*(1), 374–376. http://dx.doi.org/10.3390/rs5010374.

Asner, G.P., Jones, M.O., Martin, R.E., Knapp, D.E., & Hughes, R.F. (2008). Remote sensing of native and invasive species in Hawaiian forests. *Remote Sensing of Environment*, *112*(5), 1912–1926 (Retrieved from <Go to ISI>://000255370700002).

Asner, G.P., & Martin, R. (2008). Spectral and chemical analysis of tropical forests: Scaling from leaf to canopy levels. *Remote Sensing of Environment*, *112*(10), 3958–3970. http://dx.doi.org/10.1016/j.rse.2008.07.003.

Asner, G.P., Martin, R.E., Anderson, C.B., & Knapp, D.E. (2015). Quantifying forest canopy traits: Imaging spectroscopy versus field survey. *Remote Sensing of Environment*, *158*, 15–27. http://dx.doi.org/10.1016/j.rse.2014.11.011.

Boardman, J. (1999). Precision geocoding of low altitude AVIRIS data: Lessons learned in 1998. *Summaries of the Eighth JPL Airborne Earth Science Workshop* (pp. 63–68).

Boulesteix, A. -L., & Strimmer, K. (2006). Partial least squares: A versatile tool for the analysis of high-dimensional genomic data. *Briefings in Bioinformatics*, *8*(1), 32–44. http://dx.doi.org/10.1093/bib/bbl016.

Castro-Esau, K.L., Sanchez-Azofeifa, G.A., & Caelli, T. (2004). Discrimination of lianas and trees with leaf-level hyperspectral data. *Remote Sensing of Environment*, *90*(3), 353–372 (Retrieved from <Go to ISI>://000221308800007).

Clark, M.L., Roberts, D.A., & Clark, D.B. (2005). Hyperspectral discrimination of tropical rain forest tree species at leaf to crown scales. *Remote Sensing of Environment*, *96*(3–4), 375–398. http://dx.doi.org/10.1016/j.rse.2005.03.009.

Colgan, M., Baldeck, C., Féret, J. -B., & Asner, G.P. (2012). Mapping savanna tree species at ecosystem scales using support vector machine classification and BRDF correction on airborne hyperspectral and LiDAR data. *Remote Sensing*, *4*(12), 3462–3480. http://dx.doi.org/10.3390/rs4113462.

Congalton, R. (1991). A review of assessing accuracy of classification of remotely sensed data. *Remote Sensing of Environment*, *37*(1), 35–46.

Dalponte, M., Bruzzone, L., & Gianelle, D. (2012). Tree species classification in the Southern Alps based on the fusion of very high geometrical resolution multispectral/hyperspectral images and LiDAR data. *Remote Sensing of Environment*, *123*, 258–270. http://dx.doi.org/10.1016/j.rse.2012.03.013.

DeFries, R.S., Hansen, M., & Townshend, J. (1995). Global discrimination of land cover types from metrics derived from AVHRR pathfinder data. *Remote Sensing of Environment*, *54*(3), 209–222 (Retrieved from <Go to ISI>://A1995TN58700006).

Dennison, P. E., Halligan, K. Q., & Roberts, D. A. (2004). A comparison of error metrics and constraints for multiple endmember spectral mixture analysis and spectral angle mapper. *Remote Sensing of Environment*, *93*(3), 359–367.

Dennison, P.E., & Roberts, D.A. (2003a). Endmember selection for multiple endmember spectral mixture analysis using endmember average RMSE. *Remote Sensing of Environment*, *87*(2–3), 123–135 (Retrieved from <Go to ISI>://000186447400001).

Please cite this article as: Roth, K.L., et al., Differentiating plant species within and across diverse ecosystems with imaging spectroscopy, *Remote Sensing of Environment* (2015), http://dx.doi.org/10.1016/j.rse.2015.05.007

Dennison, P.E., & Roberts, D.A. (2003b). The effects of vegetation phenology on endmember selection and species mapping in southern California chaparral. *Remote Sensing of Environment*, *87*(2–3), 295–309. http://dx.doi.org/10.1016/j.rse.2003.07.001.

Dópido, I., Villa, A., Plaza, A.J., Member, S., & Gamba, P. (2012). A quantitative and comparative assessment of unmixing-based feature extraction techniques for hyperspectral image classification. *IEEE Journal of Selected Topics in Applied Earth Observations and Remote Sensing*, *5*(2), 421–435.

Du, Q. (2007). Modified Fisher's linear discriminant analysis for hyperspectral imagery. *IEEE Geoscience and Remote Sensing Letters*, *4*(4), 503–507.

Dudley, K. L., Dennison, P. E., Roth, K. L., Roberts, D. A., & Coates, A. R. (in press). A multi-temporal spectral library approach for mapping vegetation species across spatial and temporal phenological gradients. Remote Sensing of Environment.

Féret, J. -B., & Asner, G.P. (2012a). Semi-supervised methods to identify individual crowns of lowland tropical canopy species using imaging spectroscopy and LiDAR. *Remote Sensing*, *4*(12), 2457–2476. http://dx.doi.org/10.3390/rs4082457.

Féret, J. -B., & Asner, G.P. (2012b). Tree species discrimination in tropical forests using airborne imaging spectroscopy. *IEEE Transactions on Geoscience and Remote Sensing*, 1–12. http://dx.doi.org/10.1109/TGRS.2012.2199323.

Fisher, R.A. (1936). The use of multiple measurements in taxonomic problems. *Annals of Eugenics*, *7*(2), 179–188. http://dx.doi.org/10.1111/j.1469-1809.1936.tb02137.x.

Franklin, S.E. (1994). Discrimination of sub-alpine forest species and canopy density using digital Casi, Spot Pla, and Landsat Tm Data. *Photogrammetric Engineering and Remote Sensing*, *60*(10), 1233–1241 (Retrieved from <Go to ISI>://A1994PQ57600005).

Friedl, M. a., Sulla-Menashe, D., Tan, B., Schneider, A., Ramankutty, N., Sibley, A., et al. (2010). MODIS Collection 5 global land cover: Algorithm refinements and characterization of new datasets. *Remote Sensing of Environment*, *114*(1), 168–182. http://dx.doi.org/10.1016/j.rse.2009.08.016.

Gong, P., Pu, R.L., & Yu, B. (1997). Conifer species recognition: An exploratory analysis of in situ hyperspectral data. *Remote Sensing of Environment*, *62*(2), 189–200 (Retrieved from http://www.sciencedirect.com/science/article/B6V6V-3SWR0WD-6/2/d3c10134594795b08ea3a2502b8daed8).

Goodenough, D.G., Li, J., Asner, G.P., Schaepman, M., Ustin, S.L., & Dyk, A. (2006). Combining hyperspectral remote sensing and physical modeling for applications in land ecosystems. *2006 IEEE International Symposium on Geoscience and Remote Sensing*, *vol. 00*. (pp. 2000–2004). Ieee. http://dx.doi.org/10.1109/IGARSS.2006.518.

Green, R.O., Eastwood, M.L., Sarture, C.M., Chrien, T.G., Aronsson, M., Chippendale, B.J., et al. (1998). Imaging spectroscopy and the Airborne Visible Infrared Imaging Spectrometer (AVIRIS). *Remote Sensing of Environment*, *65*(3), 227–248 (Retrieved from <Go to ISI>://000075524700001).

Hatala, J. A., Crabtree, R.L., Halligan, K.Q., & Moorcroft, P.R. (2010). Landscape-scale patterns of forest pest and pathogen damage in the Greater Yellowstone Ecosystem. *Remote Sensing of Environment*, *114*(2), 375–384. http://dx.doi.org/10.1016/j.rse.2009.09.008.

He, K.S., Rocchini, D., Neteler, M., & Nagendra, H. (2011). Benefits of hyperspectral remote sensing for tracking plant invasions. *Diversity and Distributions*, *17*(3), 381–392. http://dx.doi.org/10.1111/j.1472-4642.2011.00761.x.

Hunt, E.R., & Williams, A.E.P. (2006). Detection of flowering leafy spurge with satellite multispectral imagery. *Rangeland Ecology & Management*, *59*(5), 494–499 (Retrieved from <Go to ISI>://000240928300007).

HyspIRI Team (2009). *NASA 2008 HyspIRI White Paper and Workshop Report*. Pasadena, CA: NASA Jet Propulsion Laboratory.

Indahl, U.G., Liland, K.H., & Naes, T. (2009). Canonical partial least squares—A unified PLS approach to classification and regression problems. *Journal of Chemometrics*, *23*(9), 495–504. http://dx.doi.org/10.1002/cem.1243.

Isaksson, A., Wallman, M., Göransson, H., & Gustafsson, M. G. (2008). Cross-validation and bootstrapping are unreliable in small sample classification. *Pattern Recognition Letters*, *29*(14), 1960–1965.

Jones, T.G., Coops, N.C., & Sharma, T. (2010). Assessing the utility of airborne hyperspectral and LiDAR data for species distribution mapping in the coastal Pacific Northwest, Canada. *Remote Sensing of Environment*, *114*(12), 2841–2852. http://dx.doi.org/10.1016/j.rse.2010.07.002.

Kalacska, M.R., Bohlman, S.A., Sanchez-Azofeifa, G.A., Castro-Esau, K., & Caelli, T. (2007). Hyperspectral discrimination of tropical dry forest lianas and trees: Comparative data reduction approaches at the leaf and canopy levels. *Remote Sensing of Environment*, *109*(4), 406–415 (Retrieved from <Go to ISI>://000248293300002).

Kampe, T. U., Johnson, B. R., Kuester, M., & Keller, M. (2010). NEON: the first continental-scale ecological observatory with airborne remote sensing of vegetation canopy biochemistry and structure. *Journal of Applied Remote Sensing*, *4*, 1–24.

Kim, S., Magnani, A., & Boyd, S. (2005). Robust fisher discriminant analysis. *Conference Proceedings of Advances in Neural Information Processing Systems*, 659–666.

Klecka, W. (1980). *Discriminant analysis*. SAGE University Press.

Kokaly, R.F., Asner, G.P., Ollinger, S.V., Martin, M.E., & Wessman, C.A. (2009). Characterizing canopy biochemistry from imaging spectroscopy and its application to ecosystem studies. *Remote Sensing of Environment*, *113*(Supplement 1), S78–S91. http://dx.doi.org/10.1016/j.rse.2008.10.018.

Kyriakidis, P.C., & Dungan, J.L. (2001). A geostatistical approach for mapping thematic classification accuracy and evaluating the impact of inaccurate spatial data on ecological model predictions. *Environmental and Ecological Statistics*, *8*(4), 311–330 (Retrieved from <Go to ISI>://000172102500003).

Li, L., Ustin, S.L., & Lay, M. (2005). Application of multiple endmember spectral mixture analysis (MESMA) to AVIRIS imagery for coastal salt marsh mapping: A case study in China Camp, CA, USA. *International Journal of Remote Sensing*, *26*(23), 5193–5207 (Retrieved from <Go to ISI>://000234504800004).

Martin, M.E., Newman, S.D., Aber, J.D., & Congalton, R.G. (1998). Determining forest species composition using high spectral resolution remote sensing data. *Remote Sensing of Environment*, *65*(3), 249–254 (Retrieved from <Go to ISI>://000075524700002).

Martin, M.E., Plourde, L.C., Ollinger, S.V., Smith, M.L., & McNeil, B.E. (2008). A generalizable method for remote sensing of canopy nitrogen across a wide range of forest ecosystems. *Remote Sensing of Environment*, *112*(9), 3511–3519. http://dx.doi.org/10.1016/j.rse.2008.04.008.

Meentemeyer, R.K., Moody, A., & Franklin, J. (2001). Landscape-scale patterns of shrub-species abundance in California chaparral — The role of topographically mediated resource gradients. *Plant Ecology*, *156*(1), 19–41 (Retrieved from http://dx.doi.org/10.1023/A:1011944805738).

Ouyang, Z. -T., Gao, Y., Xie, X., Guo, H. -Q., Zhang, T. -T., & Zhao, B. (2013). Spectral discrimination of the invasive plant *Spartina alterniflora* at multiple phenological stages in a saltmarsh wetland. *PLoS One*, *8*(6), e67315. http://dx.doi.org/10.1371/journal.pone.0067315.

Plourde, L.C., Ollinger, S.V., Smith, M.L., & Martin, M.E. (2007). Estimating species abundance in a northern temperate forest using spectral mixture analysis. *Photogrammetric Engineering and Remote Sensing*, *73*(7), 829–840 (Retrieved from <Go to ISI>://000249438300013).

Pu, R.L. (2009). Broadleaf species recognition with in situ hyperspectral data. *International Journal of Remote Sensing*, *30*(11), 2759–2779 (Retrieved from <Go to ISI>://000267263000003).

Pu, R.L., & Gong, P. (2000). Band selection from hyperspectral data for conifer species identification. *Geographic Information Sciences*, *6*(2), 137–142.

Pu, R.L., & Gong, P. (2011). Hyperspectral remote sensing of vegetation bioparameters. In Q. Weng (Ed.), *Advances in environmental remote sensing: Sensors, algorithms, and applications* (pp. 101–142). CRC Press.

Riano, D., Chuvieco, E., Ustin, S.L., Zomer, R., Dennison, P.E., Roberts, D.A., et al. (2002). Assessment of vegetation regeneration after fire through multitemporal analysis of AVIRIS images in the Santa Monica Mountains. *Remote Sensing of Environment*, *79*(1), 60–71 (Retrieved from <Go to ISI>://000172880500007).

Richter, R., & Schläpfer, D. (2002). Geo-atmospheric processing of airborne imaging spectrometry data. Part 2: Atmospheric/topographic correction. *International Journal of Remote Sensing*, *23*(13), 2631–2649. http://dx.doi.org/10.1080/01431160110115834.

Roberts, D.A., Gamon, J.A., Keightley, K., & Prentiss, D. (1999). AVIRIS Land surface mapping in support of the BOReal Ecosystem-Atmosphere Study (BOREAS). *Proceedings of the 8th AVIRIS Earth Science Workshop* (pp. 355–364). Pasadena, CA: JPL.

Roberts, D.A., Gardner, M., Church, R., Ustin, S.L., Scheer, G., & Green, R. (1998). Mapping chaparral in the Santa Monica Mountains using multiple endmember spectral mixture models. *Remote Sensing of Environment*, *65*(3), 267–279. http://dx.doi.org/10.1016/S0034-4257(98)00037-6.

Roberts, D.A., Green, R.O., & Adams, J.B. (1997). Temporal and spatial patterns in vegetation and atmospheric properties from AVIRIS. *Remote Sensing of Environment*, *62*(3), 223–240 (Retrieved from <Go to ISI>://A1997YD92900003).

Roberts, D. A., Quattrochi, D., Hulley, G. C., Hook, S. J., & Green, R. O. (2012). Synergies between VSWIR and TIR data for the urban environment: An evaluation of the potential for the Hyperspectral Infrared Imager (HyspIRI) Decadal Survey mission. *Remote Sensing of Environment*, *117*, 83–101.

Roberts, D.A., Smith, M.O., & Adams, J.B. (1993). Green vegetation, nonphotosynthetic vegetation, and soils in Aviris data. *Remote Sensing of Environment*, *44*(2–3), 255–269 (Retrieved from <Go to ISI>://A1993LB11800010).

Roberts, D. A., Ustin, S. L., Ogunjemiyo, S., Greenberg, J., Dobrowski, S., Chen, J., & Hinckley, T. (2004). Spectral and structural measures of Northwest forest vegetation at leaf to landscape scales. *Ecosystems*, *7*(5), 545–562.

Rocchini, D., Foody, G.M., Nagendra, H., Ricotta, C., Anand, M., He, K.S., et al. (2013). Uncertainty in ecosystem mapping by remote sensing. *Computers & Geosciences*, *50*, 128–135. http://dx.doi.org/10.1016/j.cageo.2012.05.022.

Rosso, P.H., Ustin, S.L., & Hastings, A. (2005). Mapping marshland vegetation of San Francisco Bay, California, using hyperspectral data. *International Journal of Remote Sensing*, *26*(23), 5169–5191 (Retrieved from <Go to ISI>://000234504800003).

Roth, K.L., Dennison, P.E., & Roberts, D.A. (2012). Comparing endmember selection techniques for accurate mapping of plant species and land cover using imaging spectrometer data. *Remote Sensing of Environment*, *127*, 139–152. http://dx.doi.org/10.1016/j.rse.2012.08.030.

Sasser, C., Visser, J., Mouton, E., Linscombe, J., & Hartley, S. (2008). *Vegetation types in coastal Louisiana in 2007*.

Schaaf, A.N., Dennison, P.E., Fryer, G.K., Roth, K.L., & Roberts, D.A. (2011). Mapping plant functional types at multiple spatial resolutions using imaging spectrometer data. *GIScience and Remote Sensing*, *48*(3), 324–344.

Serbin, S.P., Dillaway, D.N., Kruger, E.L., & Townsend, P. a. (2012). Leaf optical properties reflect variation in photosynthetic metabolism and its sensitivity to temperature. *Journal of Experimental Botany*, *63*(1), 489–502. http://dx.doi.org/10.1093/jxb/err294.

Somers, B., & Asner, G.P. (2012). Hyperspectral time series analysis of native and invasive species in Hawaiian rainforests. *Remote Sensing*, *4*(12), 2510–2529. http://dx.doi.org/10.3390/rs4092510.

Somers, B., & Asner, G.P. (2013). Invasive species mapping in Hawaiian rainforests using multi-temporal hyperion spaceborne imaging spectroscopy. *IEEE Journal of Selected Topics in Applied Earth Observations and Remote Sensing*, *6*(2), 351–359. http://dx.doi.org/10.3390/rs4092510.

Suzuki, Y., Okamoto, H., Takahashi, M., Kataoka, T., & Shibata, Y. (2012). Mapping the spatial distribution of botanical composition and herbage mass in pastures using hyperspectral imaging. *Grassland Science*, *58*(1), 1–7. http://dx.doi.org/10.1111/j.1744-697X.2011.00239.x.

Swatantran, A., Dubayah, R., Roberts, D.A., Hofton, M., & Blair, J.B. (2011). Mapping biomass and stress in the Sierra Nevada using lidar and hyperspectral data fusion. *Remote Sensing of Environment*, *115*(11), 2917–2930. http://dx.doi.org/10.1016/j.rse.2010.08.027.

The Mathworks Inc. (2012). *MATLAB and Statistics Toolbox*. (Natick, MA).

Please cite this article as: Roth, K.L., et al., Differentiating plant species within and across diverse ecosystems with imaging spectroscopy, *Remote Sensing of Environment* (2015), http://dx.doi.org/10.1016/j.rse.2015.05.007

Underwood, E.C., Mulitsch, M.J., Greenberg, J.A., Whiting, M.L., Ustin, S.L., & Kefauver, S.C. (2006). Mapping invasive aquatic vegetation in the Sacramento–San Joaquin Delta using hyperspectral imagery. *Environmental Monitoring and Assessment*, *121*(1–3), 47–64 (Retrieved from <Go to ISI>://000241453500004).

Ustin, S.L., & Gamon, J.A. (2010). Remote sensing of plant functional types. *New Phytologist*, *186*(4), 795–816. http://dx.doi.org/10.1111/j.1469-8137.2010.03284.x.

Ustin, S.L., Roberts, D.A., Gamon, J.A., Asner, G.P., & Green, R.O. (2004). Using imaging spectroscopy to study ecosystem processes and properties. *BioScience*, *54*(6), 523. http://dx.doi.org/10.1641/0006-3568(2004)054[0523:UISTSE]2.0.CO;2.

Vaiphasa, C., Ongsomwang, S., Vaiphasa, T., & Skidmore, A. (2005). Tropical mangrove species discrimination using hyperspectral data: A laboratory study. *Estuarine, Coastal and Shelf Science*, *65*(1–2), 371–379. http://dx.doi.org/10.1016/j.ecss.2005.06.014.

Van Aardt, J., & Wynne, R.H. (2001). Spectral separability among six southern tree species. *Photogrammetric Engineering and Remote Sensing*, *67*(12), 1367–1375 (Retrieved from <Go to ISI>://000172525800005).

Van Aardt, J., & Wynne, R.H. (2007). Examining pine spectral separability using hyperspectral data from an airborne sensor: An extension of field-based results. *International Journal of Remote Sensing*, *28*(1–2), 431–436 (Retrieved from <Go to ISI>://000244093200025).

Waser, L.T., & Asner, G.P. (2011). Semi-automatic classification of tree species in different forest ecosystems by spectral and geometric variables derived from Airborne Digital Sensor (ADS40) and RC30 data. *Remote Sensing of Environment*, *115*(9), 2415–2422. http://dx.doi.org/10.1016/j.rse.2011.05.004.

Wold, S., Sjostrom, M., & Eriksson, L. (2001). PLS-regression: A basic tool of chemometrics. *Chemometrics and Intelligent Laboratory Systems*, *58*, 109–130.

Yeh, C.H., & Spiegelman, C.H. (1994). Partial least squares and classification and regression trees. *Chemometrics and Intelligent Laboratory Systems*, *22*(1), 17–23. http://dx.doi.org/10.1016/0169-7439(93)E0045-6.

Youngentob, K.N., Roberts, D.A., Held, A.A., Dennison, P.E., Jia, X., & Lindenmayer, D.B. (2011). Mapping two Eucalyptus subgenera using multiple endmember spectral mixture analysis and continuum-removed imaging spectrometry data. *Remote Sensing of Environment*, *115*(5), 1115–1128 (Retrieved from http://www.sciencedirect.com/science/article/pii/S0034425710003585).

Zhai, Y., Cui, L., Zhou, X., Gao, Y., Fei, T., & Gao, W. (2013). Estimation of nitrogen, phosphorus, and potassium contents in the leaves of different plants using laboratory-based visible and near-infrared reflectance spectroscopy: Comparison of partial least-square regression and support vector machine regression met. *International Journal of Remote Sensing*, *34*(7), 2502–2518. http://dx.doi.org/10.1080/01431161.2012.746484.

Zhao, G., & Maclean, A. (2000). A comparison of canonical discriminant analysis and principal component analysis for spectral transformation. *Photogrammetric Engineering and Remote Sensing*, *66*(7), 841–847.

Zomer, R.J., Trabucco, A., & Ustin, S.L. (2009). Building spectral libraries for wetlands land cover classification and hyperspectral remote sensing. *Journal of Environmental Management*, *90*(7), 2170–2177 (Retrieved from <Go to ISI>://000266740000007).

Please cite this article as: Roth, K.L., et al., Differentiating plant species within and across diverse ecosystems with imaging spectroscopy, *Remote Sensing of Environment* (2015), http://dx.doi.org/10.1016/j.rse.2015.05.007